Optimising the *in vitro* and *in vivo* performance of oral cocrystal formulations via spray coating

Dolores R. Serrano[a,b,c*], David Walsh[a,b], Peter O'Connell[a], Naila A. Mugheirbi[d], Zelalem Ayenew Worku[a,b], Francisco Bolas-Fernandez[c], Carolina Galiana[e], Maria Auxiliadora Dea-Ayuela[e], Anne Marie Healy[a,b*]

[a]School of Pharmacy and Pharmaceutical Sciences, Trinity College Dublin, Dublin 2, Ireland.
[b]SSPC, Synthesis and Solid State Pharmaceutical Centre, Ireland.
[c]School of Pharmacy, Universidad Complutense de Madrid, Plaza Ramón y Cajal s/n, 28040-Madrid, Spain.
[d]Department of Industrial and Physical Pharmacy, Purdue University, West Lafayette, IN 47907-2091, USA.
[e]Departamento de Farmacia, Facultad de Ciencias de la Salud, Universidad CEU Cardenal Herrera, Edificio Seminario s/n, 46113-Moncada, Valencia, Spain.

*Corresponding authors:
Dolores R. Serrano
Department of Pharmaceutical Technology
School of Pharmacy
Universidad Complutense de Madrid
Plaza Ramon y Cajal s/n
28040-Madrid, Spain.
Email: drserran@ucm.es

Anne Marie Healy
School of Pharmacy and Pharmaceutical Sciences
Trinity College Dublin
Dublin 2, Ireland.
Tel.: +353 1 896 1444;
E-mail address: healyam@tcd.ie

Abstract

Engineering of pharmaceutical cocrystals is an advantageous alternative to salt formation for improving the aqueous solubility of hydrophobic drugs. Although, spray drying is a well-established scale-up technique in the production of cocrystals, several issues can arise such as sublimation or stickiness due to low glass transition temperatures of some organic molecules, making the process very challenging. Even though, fluidised bed spray coating has been successfully employed in the production of amorphous drug-coated particles, to the best of our knowledge, it has never been employed in the production of cocrystals. The feasibility of this technique was proven using three model cocrystals: sulfadimidine (SDM)/4-aminosalicylic acid (4ASA), sulfadimidine/nicotinic acid (NA) and ibuprofen (IBU)/ nicotinamide (NAM). Design of experiments were performed to understand the critical formulation and process parameters that determine the formation of either cocrystal or coamorphous systems for SDM/4ASA. The amount and type of binder played a key role in the overall solid state and *in vitro* performance characteristics of the cocrystals. The optimal balance between high loading efficiencies and high degree of crystallinity was achieved only when a binder: cocrystal weight ratio of 5:95 or 10:90 was used. The cocrystal coated beads showed an improved *in vitro-in vivo* performance characterised by: (i) no tendency to aggregate in aqueous media compared to spray dried formulations, (ii) enhanced *in vitro* activity (1.8-fold greater) against *S. aureus*, (iii) larger oral absorption and bioavailability (2.2-fold higher C_{max}), (iv) greater flow properties and (v) improved chemical stability than cocrystals produced by other methods derived from the morphology and solid nature of the starter cores.

Keywords: cocrystal, fluidised bed, beads, spray coating, sulfadimidine, pellets, ASAP, amorphous, controlled release.

Graphical abstract

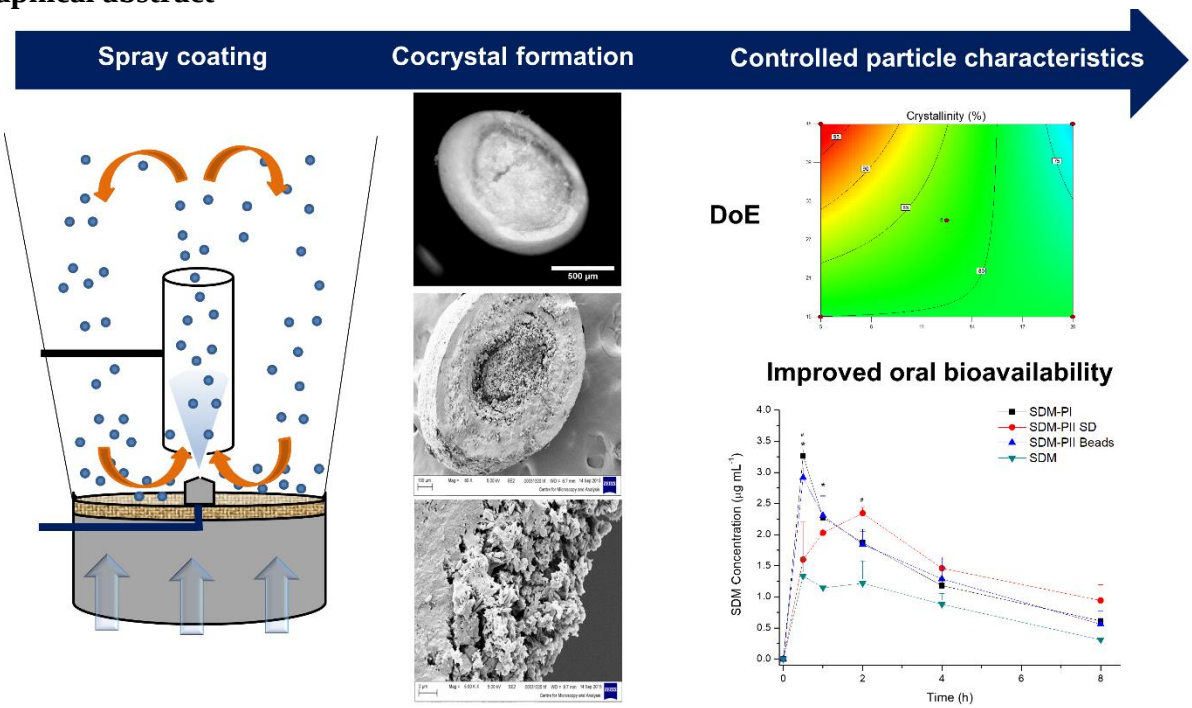

1. Introduction

The oral administration of medicines is the preferred route, with over 80% of drugs sold as tablets [1, 2]. However, the percentage of drug candidates in the R&D pipeline with low aqueous solubility is approximately 80-90% [1, 3]. For this reason, low aqueous solubility is a major concern during drug development, as it has a major impact on drug absorption and bioavailability [1, 4]. Inexpensive pharmaceutical approaches are required to make new drugs of high pharmaceutical quality affordable. Salt formation is a feasible strategy to enhance the solubility of active pharmaceutical ingredients (APIs) that contain ionisable functional groups. However, this option is not available for all APIs.

Engineering of pharmaceutical cocrystals can be an advantageous alternative to salt formation for increasing API aqueous solubility. There is no need to break or create covalent bonds because cocrystal formation is based on the hydrogen bonding interaction between the API and the coformer [5]. The coformer should be a GRAS (generally regarded as safe) listed molecule with high solubility, but it can be also be another active molecule that enhances the activity of the API. Several examples are described in the literature where the coformer improves API activity such as the sulfadimidine (SDM) - 4 aminosalicylic acid (4ASA) cocrystal for infectious diseases [6, 7] or the celecoxib - tramadol (hydrochloride) cocrystal which is used for the treatment of pain, and was recently approved and commercialized by Esteve S.A [8, 9].

Common strategies to produce cocrystals in the pharmaceutical industry are grinding and crystallisation methods. But to choose a suitable coformer is not the only crucial parameter to bear in mind. Different manufacturing processes can lead to the formation of different polymorphic forms and crystal habits, which can influence the overall dissolution and tabletting behaviour of the cocrystal. Spray drying, a well-established scale-up technique, has been shown to be a successful approach to obtain pure cocrystals [10]. Even though cocrystals produced by spray-drying are usually spherical with smaller particle size than those obtained by other techniques such as grinding, it has been reported that spray dried cocrystal powders, at least in some instances, can exhibit a higher tendency to form aggregates in aqueous media because more hydrophobic surfaces are exposed to the media, leading to limited dissolution rates [7, 11]. For this reason, cocrystals obtained by spray-drying are not always suitable in terms of physicochemical properties and *in vitro/in vivo* performance.

Fluidised bed spray coating has been successfully employed in the formation of drug-coated beads with enhanced dissolution properties and oral bioavailability [12]. One example is Sporanox® which consists of an amorphous solid dispersion of itraconazole and hypromellose coated on sugar spheres [13]. However, to the best of our knowledge, this technique has not been employed in the production of cocrystal-coated non-pareil beads.

The hypothesis underpinning this work is that fluidised bed spray coating can be used to form *in situ* cocrystals deposited as a thin layer on different substrates such as non-pareil sugar beads, resulting in particulates that are large enough to avoid aggregation in liquid medium, while improving dissolution and oral bioavailability. Quality-by design (QbD) experiments (Taguchi and Box Behnken) were performed to understand the effect of different parameters such as spray rate, air flow rate, nozzle air pressure, size and composition of the starter cores and amount and type of binder excipient on cocrystal formation during fluidised bed spray coating. The feasibility of this technique was assessed with different cocrystals: sulfadimidine/4-aminosalicylic acid, sulfadimidine/nicotinic acid (NA) and ibuprofen (IBU)/nicotinamide (NAM). The optimised cocrystal-coated beads were further evaluated and characterised for drug loading, stability, flow properties, dissolution, *in vitro* activity and *in vivo* pharmacokinetics.

2. Materials and methods

2.1. Materials

SDM, 4ASA and NAM with a purity ≥ 99%, were purchased from Sigma–Aldrich (Wicklow, Ireland). NA and IBU with a purity ≥ 99.5% were purchased from Fluka BioChemika (Wicklow, Ireland) and Kemprotec (Cumbria, UK) respectively. Inulin Frutafit® HD with an average degree of polymerisation of 10 was a gift from Sensus (Roosendaal, The Netherlands). Ethanol and acetone were supplied from Corcoran Chemicals (Dublin, Ireland). Non-pareil Seeds (sugar beads) with different particle size ranging from 250-180, 500-425 and 1000-850 µm were a gift from JRS Pharma (Rosenberg, Germany). Neutral starter cores, Cellets® (pellets made of microcrystalline cellulose) and functional starter cores, TAP® (pellets made of tartaric acid) were a gift from Pharmatrans Sanaq AG (Allschwi, Switzerland). HPLC grade methanol was purchased from Fisher Scientific (Dublin, Ireland). Potassium hydrogen phosphate was obtained from Sigma–Aldrich (Wicklow, Ireland) and phosphoric acid from Merck (Darmstadt, Germany). Polyvinylpyrrolidone (PVP K90) was a gift from BASF

(Ludwigshafen, Germany). HMPC AS LG was a gift from Shin-Etsu Chemical Co (Tokyo, Japan). Eudragit L100-55 was a gift from Evonik (Darmsdat, Germany).

2.2. Methods

2.2.1. Design of experiments

Defining the target product profile (TPP) and identifying the critical quality attributes (CQAs)

The target product profile (TPP) is primarily based on the dynamic summary of the characteristics of the drug product, as it relates to quality, efficacy and safety [14]. Considering cocrystal-coated beads as the target formulation for enhancing the solubility and activity of the API, among the TPP elements that define the key quality characteristics are: dosage form, route of administration, dosage type, pharmacokinetics, packaging and stability requirements (Table S1, supplementary material). In order to meet the TPP, various CQAs were identified as critical, such as loading efficiency, content uniformity, drug release and level of crystallinity (taking into account that amorphous domains could be also formed during spray coating) (Table S2, supplementary material).

Factor screening studies

A seven-factor eight-run Taguchi design (L2^7) was employed for factor screening studies for identifying the formulation and process variables critically influencing the product quality. In order to select the most influential variables, an Ishikawa fish-bone diagram was designed to structure the risk operation for determining the causes and sub-causes affecting the CQAs (Figure S1, supplementary material) [15]. Seven factors and two levels of each factor affecting the cocrystal-coating process were selected (Table 1). Seven factors were numerical (i - vi) and one categorical (vii):

i) Spray rate of feed solution: 0.4 (1.6 g/min) or 0.6 (2.5 g/min);
ii) Nitrogen flow rate: 25 or 35 m^3/h;
iii) Atomisation pressure: 0.7 or 1 bar;
iv) Non-pareil sugar bead size: 500 or 1000 μm;
v) Amount of sprayed mass onto the beads: 30 or 50%;
vi) Amount of binder: 1 or 5%
vii) Type of binder: inulin or PVP K90.

A total of eight formulations were prepared. Non-pareil sugar starter cores (either 500 or 1000 μm) were coated with an ethanolic solution containing the binder and SDM and 4ASA in a 1:1 molar ratio. The cocrystal components were initially dissolved in ethanol at a concentration of 1% and then the corresponding binder was added to the mixture at a concentration of either 1% or 5%. The ethanolic solution was sprayed using a fluidised bed coater equipped with a Wurster insert (Mini-Glatt, Glatt®, Binzen, Germany). The process parameters were as follow: 60°C inlet temperature, 0.5 mm nozzle diameter, 1.6 or 2.5 g/min spray rate, 25 or 35 m^3/h nitrogen flow rate and 0.7 or 1 bar atomisation pressure. Once the ethanolic solution was sprayed, the coated beads were dried inside the fluidised bed until the product temperature reached 40°C. Three responses were evaluated: degree of crystallinity, loading efficiency and attrition (expressed as a percentage of intact beads that remained after the coating process). In order to quantify the loading efficiency (LE), a known amount of coated beads were weighed, dissolved in ethanol and analysed by HPLC using a method previously described [11]. In order to account for the percentage of binder, the degree of crystallinity (DC) was calculated taking into consideration the actual percentage of cocrystal that was coated on the beads (LE) measured by HPLC and the heat of fusion (J/g) corresponding to the melting of the cocrystal at 161 °C. The heat of fusion of the cocrystal coated on beads was compared with the heat of fusion of the cocrystal prepared by solvent evaporation (SE) calculated from a 10°C/min standard DSC scan (Eq. 1) [11].

$$DC\ (\%) = \frac{\Delta Hf\ cocrystal\ coated\ on\ beads}{(LE(\%) * \Delta Hf\ cocyrstal\ SE)/100} * 100 \qquad \text{(Eq. 1)}$$

Design Expert® software version 10.0 (M/s Stat-Ease, Minneapolis, USA) was used to develop polynomial models which were analysed to delineate the main effects for each CQA through Pareto charts.

QbD-based formulation optimization studies

Based on the preliminary studies (Factor screening studies), the critical material attributes that affected the spray coating process were identified. A Box-Behnken design was then employed for systematic optimization using Design Expert® software. The central point (0, 0, 0) was studied in quintuplicate. Three factors and three levels of each factor affecting the cocrystal coating process were selected: atomisation pressure (0.6, 0.8 and 1 bar), the amount of sprayed mass onto the beads (15, 30 and 45%) and the amount of binder (5, 12.5 and 20%). The remainder of the process and formulation parameters were kept constant: 500 μm sugar bead

size, 25 m^3/h nitrogen flow rate, 60 °C inlet temperature, PVP K90 as a binder, 0.5 mm nozzle diameter and 2.5 g/min spray rate. Five responses were evaluated: degree of crystallinity, loading efficiency and attrition (expressed as a percentage of broken beads that occur during the process), content uniformity (RSD) and yield. Table 2 summarizes the experimental design matrix of the seventeen experimental runs and their factor combinations and responses.

Search for optimum formulation and validation studies

Mathematical modelling was carried out by multiple linear regression analysis (MLRA). Only the statistically significant coefficients ($p < 0.05$) were considered in framing the polynomial equations, and the model was evaluated by analysing the p-value, coefficient of correlation (R^2) and predicted residual sum of squares (PRESS). Response surface analysis was carried out employing 2D and 3D plots for understanding the relationship among the different factors on the responses. The prognosis of the optimum formulation was conducted by numerical optimization and desirability function. Validation of the QbD methodology was conducted by comparing the predicted responses with the observed ones with the help of linear correlation and residual plots [14].

2.2.2. Investigation of other formulation and process parameters in cocyrstal formation through spray coating

Effect of concentration and type of binder

After completion of the DoE studies, an optimised cocrystal formulation with maximised loading efficiency (22%) and degree of crystallinity (96%) was developed. A 5 g-batch was prepared as follows: 500 µm non-pareil sugar starter cores (2.75 g) were coated with an ethanolic solution (225 ml) containing 5% PVP K90 (0.1125 g) and 95% cocrystal components consisting of 1.375 g of SDM and 0.758 g of 4ASA. The ethanolic solution was sprayed using the following process parameters: inlet temperature of 60°C, 0.5 mm nozzle diameter, 2.5 g/min spray rate, 25 m^3/h nitrogen flow rate and 0.75 bar atomisation pressure.

In order to fully understand the process of cocrystal formation during spray coating, several formulation parameters were investigated in more detail. A range of experiments were performed preparing ethanolic solutions containing different ratios of PVP K90: cocrystal components (0:100, 5:95, 10:90, 20:80, 30:70, 40:60 and 50:50, w:w) in order to study the effect of binder concentration on cocrystal formation. Consequently, the effect of different binders (PVP K90, Inulin, Eudragit L100-55 and HPMC AS) was investigated keeping the

ratio of binder to cocrystal constant, at 10:90, and spraying onto 500 µm non-pareil sugar beads. The optimised process parameters were not modified.

Effect of particle size and composition of the starter cores

The effect of three different particle sizes (1000, 500 and 250 µm) of non-pareil sugar beads and three different compositions (sugar, microcrystalline cellulose and tartaric acid) of 500 µm starter cores was evaluated. A 5% PVP K90: 95% cocrystal ratio was employed in all the cases. The optimised process parameters were kept constant.

Effect of the batch size

The same experiments as above described for different particle size and composition of starter cores were performed using a batch size of 25 g. Binder and cocrystal components were increased proportionally compared to those employed in the 5 g batch. The optimised process parameters were kept constant.

2.2.3. Investigation of spray coating in the generation of other cocrystals

The feasibility of using spray coating to generate other cocrystals was tested using as the following examples: i) SDM/NA and ii) IBU/NAM cocrystals. The first system (SDM/NA) was prepared by dissolving the cocrystal components in 1:1 molar ratio in ethanol at 1% concentration followed by the addition of PVP K90 into the solution in a 5:95, PVP K90: cocrystal weight ratio. The solution was sprayed onto 500 µm microcrystalline beads using the optimised process parameters described above. The second system (IBU/NAM) was prepared by dissolving both cocrystal components in 1:1 molar ratio in acetone at 3% concentration. Then, Eudragit L100-55 was added into the solution in a 10:90, Eudragit:cocrystal weight ratio. The solution was sprayed onto non-pareil sugar beads using the following process parameters: temperature of 50 °C, 0.5 mm nozzle diameter, 2 g/min spray rate, 35 m^3/h nitrogen flow rate and 0.7 bar atomisation pressure.

For comparison purposes, cocrystals were also produced by spray drying and/or solvent evaporation as previously described [6, 16]. A physical mixture of the single components was prepared using a mortar and pestle.

2.2.4. Physicochemical characterisation

Modulated temperature DSC (MTDSC)

MTDSC scans were recorded on a QA-200 TA instrument (TA instruments, Elstree, United Kingdom) calorimeter using nitrogen as the purge gas. Intact beads were weighed (4-6 mg) and sealed in closed aluminium pans with one pin-hole. A scanning rate of 5 °C/min, amplitude of modulation of 0.796 °C and modulation frequency of 1/60 Hz were employed. The temperature range was from 25 °C to 210 °C [17]. Calibration of the instrument was carried out using indium as standard. Temperatures of melting events (n = 3) refer to onset temperatures.

Thermogravimetric analysis (TGA)

Thermogravimetric analysis (TGA) was performed using a Mettler TG 50 module (Greifensee, Switzerland). Samples were placed in open aluminum pans (2-6 mg) and analysed at a constant heating rate of 10°C/min between a temperature range of 25 °C and 250 °C.

Dynamic Vapour Sorption (DVS)

Water sorption kinetic profiles were obtained using a DVS (Advantage, Surface Measurement Systems, Alperton, UK) at 25.0 ± 0.1°C. Water was used as the probe vapour. Samples were dried at 0% relative humidity (RH) for 1 h and then subjected to step changes of 10% RH up to 90% RH, and the reverse for desorption. The sample mass was allowed to reach equilibrium, defined as dm/dt ≤ 0.002 mg/min over 10 min, before the RH was changed [6, 18]. Sample weights were between 15 and 20 mg.

Imaging

The surface morphology of the beads, previously coated with gold/palladium, was evaluated using scanning electron microscopy (SEM). In addition, the morphology of the 1000 µm coated and uncoated non-pareil sugar beads was imaged by using a 9MP 2-200 x digital microscope (Conrad Electronics, Germany) and images were processed by Image J v1.46 image analysis software [19]. Beads were cut in half in order to see in more detail the thickness of the coating layer.

Particle size distribution analysis (PSD)

The geometric particle size distributions (PSD) were measured by laser diffraction using a Malvern Mastersizer 2000 (Malvern Instruments Ltd.Worcestershire, U.K.). Particles were dispersed using a Scirocco dry feeder instrument with 0.5 bar pressure under a vibration feed rate of 50% [11]. Taking into account the average particle size (D_{50}) before and after coating, the thickness of the coating layer was calculated as indicated in equation 2:

$$\text{Thickness} = \frac{(D50\ after\ coating - D50\ before\ coating)}{2} \quad \text{(Eq. 2)}$$

Surface area measurements

To determine the specific surface area (TBET) by the Brunauer, Emmett, Teller (BET) isotherm method, a Micromeritics Gemini VI (Micromeritics, Norcross, GA, USA) surface area analyser was used. The specific surface area of the samples was determined by the N_2 adsorption BET multipoint method, with 6 points in the relative pressure range of 0.05-0.3, using a Micromeritics Gemini 2385c (Micromeritics, Norcross, USA). Each average result was calculated on the basis of three measurements [6]. Samples were prepared by purging under N_2 overnight at 25 °C.

Flow measurements

The basic flow energy (BFE), specific energy (SE) and stability index (SI) of the beads were measured using a FT4 Powder Rheometer (Freeman Technology Ltd., Gloucestershire, UK). All tests were done in 25 g batch samples using a blade fitted within a 25- mm diameter cylinder. The material was subject to a standard conditioning cycle, to ensure that the state of each sample was reproducible before every test. The BFE and SE were measured by rotating a precision blade anti-clockwise downward and clockwise upward, respectively, in a helical path through a fixed volume of conditioned material. During the downward traverse, the torque and axial force acting on the blade were measured, and the resistance to flow was calculated and expressed as energy [20, 21].

2.2.5. Dissolution studies

Cocrystal-coated beads were weighed (200 mg) and filled into HPMC capsules size 1 (Vcaps®). Dissolution studies were performed according to USP Method I (basket method) utilising a Sotax dissolution apparatus with a rotation speed of 100 rpm. The dissolution medium was 900 ml of simulated intestinal fluid without enzymes adjusted to pH 6.8 at 37°C [22]. Samples (5 ml) without replacement were obtained at: 5, 10, 15, 20, 30, 40, 50 and 60 min. Samples were filtered through 0.45 μm filter (PVDF, Millex® HV, Merck Millipore) and analysed by HLPC as previously described [11]. For comparison purposes, dissolution studies were also performed on non-pareil sugar beads coated with SDM. SDM was dissolved in ethanol at 1% concentration and sprayed onto no –pareil sugar beads using the same process parameters as for the optimised cocrystal formulation.

2.2.6. Accelerated stability studies

The optimised SDM:4ASA cocrystal-coated beads (25 mg) were placed in uncapped HPLC vials and introduced into test chambers exposed to different conditions of temperature and humidity: 50/50, 60/30, 70/11, 70/75, 80/30, 80/50 (°C/ % RH). The desired humidity was achieved by using Amebis humidity capsules (Amebis Ltd., Ireland) which were placed into Amebis sample holders, which in turn were put inside ovens at the selected temperature in order to ensure that the RH equilibrium was reached prior to the aging of the formulations [23]. A sensor cap was used to seal the test chamber and a logger cap was connected to the sensor cap in order to collect and transmit the temperature and humidity test conditions wirelessly to the Amebis Control Software (Amebis Ltd., Ireland) every half an hour. The mean kinetic temperature and relative humidity in every condition during the experiments were calculated using Amebis Software. At different time points, samples were collected and analysed by HPLC for chemical degradation and by PXRD for solid state changes/physical degradation. Stability modelling was performed using ASAPprime® software (FreeThink Technologies Inc., Branford, CT, USA). A humidity-corrected Arrhenius equation was used to estimate the effect of temperature and RH on degradation rates (Eq.3) [24]:

$$lnK = lnA - \frac{Ea}{RT} + B\ (RH) \qquad \text{(Eq. 3)}$$

Where K is the degradation constant, A is the collision frequency, Ea is the activation energy, B(RH) is the humidity sensitivity factor, T is the absolute temperature and R is the gas constant. The method used was "potency with RH" which focuses on the remaining amount of SDM with variation in temperature and RH. Parameters selected for modelling were the following: 95% specification limit and calculated GAB (Guggenheim-Anderson-de Boer) parameters obtained from DVS isotherm plots [7]. Different fitting methods/models were assessed: Avrami, diffusion, first order, second order and zero order [25]. The model with the highest R^2 was selected for shelf life prediction at a mean kinetic temperature of 25 ℃ and 60% relative humidity.

For comparison purposes, the chemical and physical stability of the cocrystal-coated beads was compared with SDM:4ASA cocrystal generated by spray drying or milling [11] as well as a physical mixture of the single components and the SDM raw material.

2.2.7. *In vitro* antimicrobial activity

The *in vitro* activity of the different cocrystal-coated beads was evaluated against *Staphylococcus aureus* (CECT 239) as an example of Gram-positive bacteria, obtained from the Coleccion Española de Cepas tipo [26]. The antibacterial activity assay was carried out using the agar diffusion assay according to the USP Pharmacopoeia, as previously described [7], using Mueller-Hinton agar plates inoculated with a suspension (equivalent to a 0.5 McFarland standard) of the clinical isolates [7, 27]. The plates were incubated at 35 ºC for 24 hours and the growth inhibition zone diameters (mm) were carefully measured with callipers [26]. All tests were carried out in triplicate.

2.2.8. Pharmacokinetic Studies

Single oral dose administration

All experiments were performed under a Universidad Complutense Home Office Animal License. CD-1 mice were randomly split into four groups (n = 4). Animals were allowed free access to water and food throughout the study.

The optimized formulation consisting of SDM-4ASA cocrystal-coated on non-pareil sugar beads was suspended in deionized water and then administered by oral gavage at 15 and 8.3 mg/kg dose of SDM and 4ASA respectively (equivalent to 1:1 SDM:4ASA molar ratio). As a comparison, the same doses of SDM-4ASA cocrystal generated by spray drying (PII-SD) [11], milling (PI) [11] and SDM raw material were also administered. Mice were sacrificed at different time points (0.5, 1, 2, 4, and 8 h), and blood was collected from the heart in heparinized tubes. Plasma was separated by centrifugation (4500 rpm, 10 min) and stored at −40 °C until analyses were performed.

Determination of SDM and 4ASA plasma concentrations

Drugs were extracted from plasma (50 µl) using methanol (250 µl). After vortexing, the mixture was centrifuged (8000 rpm, 10 min, Hettich Universal 32 centrifuge, Tuttlingen, Germany). The supernatant (100 µl) was collected and a second extraction was performed with methanol (200 µl). Samples were centrifuged as described above and supernatants were transferred into vials and analysed by HPLC.

The concentration of SDM and 4ASA was determined using a Jasco PU-1580 pump, a Jasco AS-2050 plus autosampler and a Jasco UV-1575 UV–visible detector. Integration of the peaks

was performed with the program Borwin1.5 for PC (JMBS Developments). The mobile phase consisted of methanol/buffer pH 6.5 40/60 (v/v). The buffer was prepared from a 50-mM dipotassium phosphate solution adjusted to pH 6.5 with phosphoric acid. The mobile phase was vacuum-filtered through a 0.45 µm membrane filter (Pall Supor 0.45 µm, 47 mm) and bath-sonicated for 5 min. Compounds were separated on a 250 × 4.6 mm, 5 µm particle size Thermo Hypersil BDS C18 reverse-phase at a UV detection wavelength of 265 nm with an injection volume of 100 µl. The elution was carried out isocratically at ambient temperature with a flow rate of 1 ml/min. Calibration curves in plasma were linear for both components between 50 µg/ml and 0.02 µg/mL ($R^2 > 0.999$).

Pharmacokinetic data analysis

Non-compartmental pharmacokinetic analysis was performed using PK solver (Add-in programme in Microsoft Excel) [28, 29]. The area under the plasma concentration versus time curve (AUC) and the area under the first moment curve (AUMC) from 0-8 h were calculated using the linear trapezoidal method. The concentration at time=0 (C_{max}) was calculated by extrapolation on the y-axis of the Ln concentration (the first two plasma concentration points) versus time. The terminal phase elimination rate constant (λ) was calculated from the negative slope of Ln-linear terminal portion of the plasma concentration versus time curve. λ values were used to calculate the terminal elimination half-life ($t_{1/2}$) using equation 4:

$$t_{1/2} = \frac{0.693}{\lambda} \quad \text{(Eq. 4)}$$

The AUC and AUMC were extrapolated from last time point to infinity using equations 5 & 6, where C_{8h} is the plasma concentration at 8 h.:

$$\mathrm{AUC} = \frac{C_{8h}}{\lambda} \quad \text{(Eq. 5)}$$

$$\mathrm{AUMC} = \frac{C_{8h} \times 8}{\lambda} + \frac{C_{8h}}{\lambda^2} \quad \text{(Eq. 6)}$$

Total body clearance (Cl), volume of distribution (Vd) and mean residence time (MRT) were calculated as indicated in equation 7, 8 and 9:

$$\mathrm{Cl} = \frac{\mathrm{Dose}}{\mathrm{AUC}_{0-\infty}} \quad \text{(Eq. 7)}$$

$$\mathrm{Vd} = \frac{\mathrm{Dose}}{\lambda \times \mathrm{AUC}_{0-\infty}} \quad \text{(Eq. 8)}$$

$$\mathrm{MRT} = \frac{\mathrm{AUMC}_{0-\infty}}{\mathrm{AUC}_{0-\infty}} \quad \text{(Eq. 9)}$$

Statistical analysis

Statistical analysis was performed via one-way analysis of variance test using Minitab 17 (Minitab Ltd, Coventry, UK) followed by Tukey's test considering p-values for statistical significance <0.05 [11].

3. Results

3.1. Design of experiments (DoEs)

Preliminary screening

The screening of various process and formulation parameters was performed employing a Taguchi design for seven factors at two levels each. Implementation of the design helped in identifying the most significant factors for further detailed investigation with minimum experimentation, thus saving considerable time, effort and materials. This design has the specific advantage of requiring minimal (8) runs for a large number of independent variables (Table 1). Principally, screening embarks upon the phenomenon of "sparsity effect", i.e., only a few of the factors among numerous envisioned ones truly explain a large proportion of the experimental variation [30].

In Figure 1, Pareto charts show the most influential variables during the spray coating process. The atomisation pressure had a significant negative effect on the loading efficiency and the attrition, meaning that the higher the pressure, the lower the loading efficiency and the smaller the amount of intact beads at the end of the process. For this reason, this effect was studied in more depth in the second DoE (Box-Behnken) which included three levels. The amount of sprayed mass had an overall positive effect on the process, in particular, the higher the amount of sprayed mass, the higher the degree of crystallinity and the loading efficiency. As for the atomisation pressure, three levels of sprayed mass were established in the Box-Behnken design to explore in more detail. The nitrogen flow rate had a negative impact on the loading efficiency probably because, at higher rates, a greater percentage of sprayed solution was stuck onto the filters located at the top part of the fluidised bed coater. For this reason, the lower flow rate (25 m^3/h) was selected and kept constant in the second DoE. Lower flow rates were not tested as beads did not flow well when the flow rate was below 20 m^3/h.

Regarding the bead size, the larger size (1000 µm) resulted in a negative effect on the loading efficiency, degree of crystallinity and attrition. The reduced loading efficiency and crystallinity are a consequence of the smaller surface area available for coating compared to the 500 and 250 µm beads. Also, due to the larger size, the 1000 µm beads impact with more energy on the top of the filter, promoting attrition. For all these reasons, a 500 µm bead size was selected and kept constant in the second DoE. A smaller particle size was not included in the Box-Behnken design because, in preliminary assessments, it was observed that the electrostatic interactions of the particles were much higher when 250 µm beads were used, resulting in poor flow and sticking to the walls of the equipment and thus, high variability in the content uniformity.

The spray rate of the feed solution positively affected the degree of crystallinity and prevented attrition, so the higher spray rate (2.5 g/min) was kept constant in the next DoE. Higher spray rates were not selected because in preliminary studies it was observed that very fast rates (> 3 g/min) resulted in agglomeration of beads as the drying time was insufficient.

Regarding the amount and type of binder, no significant effect was observed, probably because the range selected was insufficient to observe differences in the responses. For this reason, the amount of binder included in the formulation was assessed in the second DoE at three different levels. Based on preliminary studies, PVP K90 was selected as the binder, as inulin promoted higher attrition levels than PVP K90.

QbD-based model development and response surface analysis

Polynomial analysis was carried out by a multilinear regression analysis method suggesting that the linear and two factor interaction models were the best fit for the parameters assessed. The coefficients of the model equations generated for each CQA (Table S3, Supplementary material) revealed goodness of fit of the experimental data to the selected model with high values of R^2 and low p-values < 0.05 for three of the responses: loading efficiency, the degree of crystallinity and yield. No significant differences were observed in the percentage of attrition and content uniformity ($p > 0.05$).

The 2D-contour plot and 3D-response surface plot depicted in Figure 2 revealed a higher influence of the amount of mass sprayed on the loading efficiency, whereas the influence of the amount of binder was found to be negligible. Higher loading efficiency was obtained when greater amounts of mass were sprayed onto the beads and also at lower atomisation pressures.

Regarding the degree of crystallization, the most influential variables were the amount of binder and sprayed mass (Figure 3). Higher values of crystallinity were achieved when low amounts of binder and high amounts of mass was sprayed. When the amount of binder was too high, the degree of crystallinity decreased significantly due to the generation of an amorphous system. The effect of the atomization pressure was found to be negligible.

In contrast, opposite effects were observed for the yield (Figure S2A, supplementary material). Yield increased significantly when higher amounts of binder were used, as it ensured the sprayed mass had a better adhesion to the beads. The atomisation pressure also played a key role in affecting yield, which was reduced when higher atomisation pressures were used due to the limited contact time of the sprayed mass with the flowing beads.

Most of the factors exhibited a negligible effect on the attrition and content uniformity ($p > 0.05$). However, it is noteworthy that high atomisation pressure promoted high attrition rates (Figure S2B, supplementary material) and low amounts of mass sprayed led to poor content uniformity (RSD > 3%) (Figure S3, Supplementary material).

Search for the optimum formulation and validation of QbD

The search for an optimum formulation was carried out by trading-off various CQAs to attain the desired objectives giving priority to maximisation of loading efficiency and degree of crystallinity. Based on the aforesaid objectives, the optimised process and formulation parameters were: 5:95, binder:cocrystal weight ratio, 45% sprayed mass and 0.75 bar as atomisation pressure, resulting in 22.1% loading efficiency and 96.2% crystallinity (Table S4, Supplementary material). Validation of the QbD methodology revealed close proximity between the predicted values of the responses with observed ones for prepared check-point formulations. (Table S5, Supplementary material). The percent prediction error for the CQAs varied between 0.76 and 1.06%, ratifying excellent goodness of fit.

3.2. Investigation of other formulation and process parameters in cocrystal formation through spray coating

The effect of other factors was investigated while keeping constant the optimised parameters from the second DoE. PXRD analysis showed that SDM:4ASA polymorph II cocrystal was successfully produced by spray coating (Figure S4, Supplementary material). Characteristic diffraction peaks at 8.7, 10.9 and 13.7 (2θ degrees) differed from those corresponding to the physical mixture of SDM and 4ASA and also from the non-pareil sugar beads but were

superimposed with the Bragg peaks of polymorph II cocrystals obtained by solvent evaporation and spray drying [6].

Results of the thermal analysis showed that the melting point of the SDM:4ASA polymorph II cocrystal coated beads was 164.5 ± 0.61 ℃ (Figure 4A) when 5% of PVPK90 was used, which differed from that of the non-pareil sugar beads (Tm = 190.5 ± 0.9 ℃). The PVPK90 concentration played a key role in the spray coating process, significantly affecting both the loading efficiency and the degree of crystallinity (Table 3 and Figure S5 in Supplementary material). A minimum percentage of the binder was required to ensure that the sprayed solution appropriately coated the beads within the fluidised bed. When no binder was used, the loading efficiency was considerably reduced. However, very high percentages of PVPK90 did not result in greater loading efficiencies, as the spray solution was extremely sticky hampering the coating process. Also, the larger the percentage of binder, the higher the depression of the melting point of the cocrystal and the lower the degree of crystallinity due to the formation of an amorphous solid dispersion (Figure 4A). The glass transitions for amorphous SDM and PVP K90 were reported to be 78 ˚C and 173 ˚C, respectively [31, 32]. No experimental glass transition has been reported for 4ASA due to its high tendency for crystallisation. After spray coating, an amorphous system could be formed due to the interaction between SDM and PVP rather than with 4ASA. At higher percentages of PVP (≥20%), evidence of a glass transition was observed in some of the systems (Figure 4A).

Regarding the type of binder (Figure 4B), HMPCAS and Eudragit L-100-55 were good alternatives to PVPK90 as their use resulted in equivalent loading efficiencies and a higher degree of crystallinity. In contrast, even though a 100% degree of crystallinity was achieved with inulin, the loading efficiency was very poor and attrition was promoted.

No differences were observed when MCC and TAP starter cores were used instead of non-pareil sugar beads in terms of loading efficiency (Figure 4C, Table 3). The degree of crystallinity was similar between sugar and MCC beads. The degree of crystallinity on TAP beads was not calculated as the melting temperature of the tartaric acid was lower than the melting of the cocrystal and then a broad peak was obtained in the DSC thermogram (Figure 4B-f).

The bead size had a significant impact on the loading efficiency and degree of crystallinity. 500 µm beads were found to be the optimal size to ensure high loading and high crystallinity.

When a larger bead size was used, the surface area available for coating was reduced and then the loading efficiency was lower. However, a smaller bead size did not improve the loading as the starter cores exhibited poor flow within the fluidised bed resulting in lower coating efficiency. When the batch size was increased from 5 to 25 g, the coating efficiency was higher (1.7-2.2-fold) but the degree of crystallinity was 7-8% lower, probably indicating that less binder is required in the manufacturing of larger batches (Figure 4D and Figure 6S, Supplementary material).

3.3. Investigation of spray coating in the generation of other cocrystals

Spray coating resulted in the formation of a single melting peak for the SDM:4ASA cocrystal which was between those of SDM (T_m = 197.1 ± 0.1 ℃) and 4ASA (T_m = 145.6 ± 0.4 ℃). However, the melting point of the non-pareil sugar beads at 190 ℃ would obscure the presence of a melting event corresponding to the SDM. For this reason, SDM:4ASA cocrystal was sprayed onto MCC beads which are amorphous in nature and do not possess any melting event at temperatures below 220 ℃. The DSC thermogram only showed a single event related to the melting of the cocrystal (Figure 5A-e). In contrast, two different melting peaks were observed in the SDM:4ASA polymorph II produced by either spray drying (Figure 5A-f) or solvent evaporation (Figure 5A-g), corresponding to the melting of the cocrystal and traces of SDM. The second melting point related to SDM is only evident when the DSC run was performed at scan speeds of 5℃/min or lower but not at 10 ℃/min (data not shown).

The production of SDM:NA cocrystal was also feasible using spray coating (Figure 5B). Similarly, for the cocrystal generated through spray drying, the melting peak was found at 203.7 ± 0.8 ℃, lying between those of SDM (T_m = 197.1 ± 0.1 ℃) and NA (T_m = 237.4 ± 0.4 ℃). The coating was performed on MCC beads for the same reason as described above.

The IBU:NAM cocrystal was also successfully produced by the fluidised bed coater (Figure 5C). A single melting peak was observed in the DSC thermogram at 88.01 ± 0.3 ℃ between the melting of the single components, 76.5 and 130.4℃ for IBU and NAM respectively. In contrast, solvent evaporation led to the generation of two melting events at 66 and 90 ℃ similarly to the physical mixture of IBU and NAM.

3.4. Physicochemical characterization

The SEM micrographs showed that the morphology of the coated beads was quasi spherical (Figure 6). At higher magnifications, the deposition of small crystals, close to 1 μm in size,

was observed (Figure 6 a1-a2). When higher percentages of PVP K90 were used (Figure 6 b-g), the beads became more non-spherical probably suggesting a non-homogeneous deposition of the cocrystal. Also, at larger magnifications, it was observed that cocrystals were embedded within a smoother matrix corresponding to the PVP (Figure 6 f2-g2). At 50% PVP concentration, the beads were agglomerated, probably being the reason why poor yield, loading efficiency and crystallinity were obtained for this batch (Figure 6g1). The higher amounts of PVP led to a lower surface area and at the same time higher residual water content which can be a disadvantage in terms of chemical stability (Table 3 and Figure S7, Supplementary material). In terms of dissolution, the presence of PVP controlled the release of SDM over time. The batch without binder exhibited the highest release (92.3%) at 15 min (Table 3 and Figure S8, Supplementary material). In all the cases, 100% release was achieved after 60 min.

The release of SDM was compared for the cocrystal and SDM coated beads. A lag time of 10 min was found in all the formulations due to the initial dissolution of the capsule shell. At earlier times, after release from the capsule (10-15 min), the dissolution rate from the cocrystal coated beads (prepared using the optimised process and formulation parameters) was 4-fold higher (Figure S9, Supplementary material), compared to the co SDM:PVP system that was generated during the spray coating process. The glass transition of the SDM:PVP amorphous system was 98.23℃ which was observed in the reversing heat flow signal during the MTDSC analysis (Figure S10B, Supplementary material). The Tg was almost 20℃ higher than the value reported for the amorphous SDM in the literature probably due to the interaction with PVP [31]. However, over the temperature range of the DSC method utilized, i.e. 25°C to 210°C, no evidence of a glass transition was found in any of the cocrystal systems when 5% of PVP was used.

Regarding the use of other types of binders, it was observed that inulin led to the most spherical particles compared to HMPCAS and Eudragit (Figure 6h-k). Even though, the system containing inulin exhibited the lowest surface area, the release of SDM at 15 min was the fastest (93.7% released at 15 minutes, which was equivalent that of the system prepared without binder), which can be related to the high water solubility of the inulin itself (Table 3, Figures S11 and S12, Supplementary material). However, as can be shown in Figure 6h1, attrition is one of the major issues related to the use of this excipient. Similarly to PVP, systems containing HPMCAS and Eudragit also exhibited a controlled release of SDM from the cocrystal coated beads at earlier time points.

In terms of particle size of the starter cores, the higher the size, the smaller the surface area and water content, but also the lower the SDM release (Table 3 and Figure S13 and S14, Supplementary material). Regarding composition, cocrystal coated on MCC beads exhibited similar characteristics (water content, surface area and SDM release) to those obtained with non-pareil sugar beads, whereas TAP beads resulted in a significantly slower SDM release, partially due to the lower surface area of the particles. It is noteworthy that the starter cores (all sizes and compositions) are very compact particles with extremely low fluidized surface areas but after the coating process, the surface area becomes between 3-5-fold higher (Table 3).

The particle size of the starter cores was found to be within the limit range stated from the suppliers. Taking into account the median particle size (D_{50}) before and after coating (Table 3), the thickness of the coating layer was estimated. The thickness of the coating layer varied between 15 to 60 µm depending on the system and was doubled when 25 g batches were prepared. These values were confirmed by optical and SEM microscopy (Figure 7). At greater magnifications (Figure 7 b3 & c3), the morphology of the coating layer can be appreciated in more detail, and consists of a porous structure of small crystals close to 1 µm in size.

The DVS sorption profiles showed a large uptake of water between 60 to 90% relative humidity for uncoated beads due to their hydrophilic nature. In contrast, the cocrystal coated beads exhibited a lower water uptake at higher relative humidity values. It is noteworthy that the greater the thickness of the coating layer, the lower the water sorption (Figure 7d and Figure S15, Supplementary material).

The flow properties of the coated and uncoated beads were also investigated (Figure 7e). Bearing in mind that the beads are intended for capsule filling, good flow is recommended in order to avoid weight variability. Cocrystal coated on non-pareil sugar beads exhibited lower SE compared to the uncoated beads, indicating that the spray coating process led to less cohesive particles than the starting beads, except for those of 1000 µm, for which a higher SE was obtained after the coating. A value of SE less than 5 mJ/g was observed in all the coated systems (except for those of 1000 µm) which is associated with less cohesive solid particles, indicating that they are suitable for acceptable capsule filling. Overall the coated beads exhibit a less cohesive behaviour with stable flow properties, indicated by SI values which were closer to unity than uncoated beads. The coated beads were also less prone or insensitive to flow rate (flow rate index *ca.* 1).

3.5. Accelerated stability studies

Accelerated stability studies indicated that all cocrystals including both polymorph I and II were less chemically stable than SDM raw material (Table 4). Among all cocrystal formulations, the one coated on beads (with optimised processing conditions and formulation) exhibited the greatest shelf life (4-fold increase) followed by the physical mixture of SDM-4ASA, spray dried polymorph II and milled polymorph I. According to the modified Arrhenius equation, the cocrystal coated beads had the highest activation energy indicating that greater energy is required to promote the chemical degradation. One of the reasons that can explain the improvement in stability is the solid nature of the cocrystal, as is attached to a solid carrier. In contrast, the other cocrystals were tested as powders and are expected to be more susceptible to moisture. In addition, both spray dried polymorph II and milled polymorph I formulations have much higher surface area (3.7 and 2.8 m^2/g respectively) and smaller particle size (D_{50} of 5.7 and 44.9 µm respectively [11]), which is likely to facilitate the interaction with moisture, promoting the degradation kinetics, compared to the cocrystal coated on beads. It is also worth noting that the chemical stability of SDM was drastically reduced in the presence of 4ASA (physical mixture). This finding can be explained by the fact that 4ASA is prone to degradation, which can trigger a faster decomposition of SDM, but also, the PXRD pattern revealed the *in situ* formation of polymorph I (which is less stable) during the stability studies especially under those conditions involving extreme relative humidity and temperature values (Figure S16, Supplementary material). PXRD patterns of the spray dried polymorph II and milled polymorph I showed the appearance of SDM Bragg peaks and reduction in the cocrystal peaks due to the degradation of 4ASA over time (Figure S17-18, Supplementary material).

3.6. *In vitro* antimicrobial activity

The coformer (4ASA) did not show antibacterial *in vitro* activity by itself. However, the physical mixture of both SDM and 4ASA increased the activity compared to the drug alone, probably because in the presence of the coformer, the aqueous solubility of the SDM was improved, which is necessary to interact with the bacteria and exert its activity by inhibiting the synthesis of dyhydrofolic acid. All cocrystal formulations exhibited significantly ($p< 0.05$) higher *in vitro* antimicrobial activity against *S. aureus* than SDM, except for those that contained Eudragit as binder, probably due to the hindered release across the agar. Among all formulations, cocrystal coated on beads with 5% PVP exhibited the greatest *in vitro* activity (1.8-fold increase) in the whole range of concentrations tested. In contrast, amorphous SDM

coated on beads with 5% PVP had less activity at lower concentrations than the drug itself, probably due to a slower release from the cores which shows an advantage of the cocrystal over the amorphous system (Figure 8A).

3.7. Pharmacokinetic profile

SDM, cocrystal polymorph I generated by milling and cocrystal coated on beads (polymorph II) exhibited a similar pharmacokinetic profile, characterised by a fast absorption at earlier times (t_{max} =30 min) followed by a fast clearance from the blood stream (Figure 8B and Table 5). The C_{max} after oral administration of polymorph I and cocrystal coated on beads was 2.5 and 2.2-fold higher respectively than SDM alone. The AUC values were also 1.65-fold higher than SDM.

The pharmacokinetic profile of cocrystal polymorph II generated by spray drying was markedly different from the cocrystal polymorph II coated on beads as well as cocrystal polymorph I. Its profile was characterised by a slower absorption phase (t_{max} =2 h) followed by a slower disappearance from plasma (2.3-fold lower than SDM) resulting in higher AUC and longer MRT than the other two cocrystal formulations.

The 4ASA exhibited similar pharmacokinetic profiles to SDM for all the formulations (Figure 8C). Lower C_{max} and AUC values were observed as a lower dose was administered taking into account the stoichiometry of the cocrystal. The major reason behind these findings may be attributed the dissolution profile of the cocrystal systems. After spray drying, the generated cocrystal powder has a high tendency to aggregate in aqueous medium, hampering the dissolution at earlier time points [7] and hence, presumably, absorption. In contrast, both polymorph I produced by milling and cocrystal coated beads have a quicker release in aqueous media resulting in a faster absorption profile.

4. Discussion

Many challenges have been described in the literature during translational development of pharmaceutical cocrystals such as: safety of the coformers, polymorphic form, solvates, hydrates, salts [33], traces of co-amorphous domains, unpredictable performance during dissolution and difficulties in establishing in vitro-in vivo correlation [34]. Most of these issues are highly dependent on the type of manufacturing process utilised to produce the cocrystal [35]. Regarding the production of the SDM:4ASA cocrystal, polymorph I was generated by a

top down approach, i.e. milling, while polymorph II was obtained using bottom up strategies such as solvent evaporation and spray drying [6]. However, this is the first time that fluidised bed spray coating has been employed in the generation of a micrometric cocrystal layer deposited on different substrates. Overall, the spray coating has allowed the formation of pure cocrystals (i.e. not contaminated with either API or coformer) compared with other techniques such as spray drying and solvent evaporation, probably because lower temperatures are required during the evaporation of the solvent and the risk of sublimation is minimised [36]. This is considered to be a major issue in the generation of certain cocrystals, such as SDM:4ASA, as 4ASA can sublime at low temperatures and then the molar ratio changes leading to a certain fraction of drug that crystallises separately [6]. Additionally, spray coating can be a useful technique for molecules with very low glass transition temperatures, such as IBU, that can cause stickiness issues during spray drying [37, 38].

The effect of many different factors that can affect the process has been explored in this work. The amount and type of binder play a key role in the overall solid state and *in vitro* characteristics of the cocrystals. The binder is necessary to ensure the appropriate deposition of the cocrystal onto the beads; however if the amount is too high, H-bonding interactions between the cocrystal components with the binder could occur and affect the integrity of the cocrystal, leading instead to an amorphous system. Predicting the miscibility of cocrystal components between themselves as well as with the carrier excipient using solubility parameters such as Hansen Solubility Parameters can guide the selection of potential coformers and binders prior to cocrystal screening [39-41].

The formation of amorphous systems during spray coating is actually one of the most common applications of using the fluidised bed to improve physicochemical properties of poorly soluble drugs [42]. However, this is a key challenge that has to be overcome in the production of cocrystals. In some cases, cocrystal formation appeared to progress via an amorphous intermediate stage which may lead to residual amorphous domains within the cocrystal lattice [43]. It has been suggested that water (a potent plasticizer) enhances the rate of cocrystallisation of these amorphous intermediate stages [44].

The optimised formulation obtained from the DoE study contains only 5% binder, as higher levels of PVP were shown to drastically reduce the crystallinity of the cocrystal. PVP K90 was included as a model binder in the DoE; nevertheless, subsequent experiments have shown that other excipients such as HMPC AS would also be suitable candidates in the production of

cocrystals through spray coating, leading to formulations with high loading and crystallinity. The use of other excipients was less successful, such as inulin which resulted in high attrition rates and poor loading efficiency, or Eudragit that led to poorer *in vitro* activity against *S. aureus*.

Regarding the starter cores, no major differences were observed in terms of composition, except the lower release rate obtained from TAP beads which may be related to a stronger interaction between the SDM and the acidic groups in the core instead of the 4ASA. However, other authors have reported significant differences in drug release depending on the composition of the core material [45-47]. As expected, the particle size of the beads has a significant effect on the physicochemical characteristics of the cocrystal. Larger sizes led to a lower surface area available for cocrystals to be deposited and also, lower dissolution rates. Coated beads with smaller particle size exhibited faster dissolution rates due to the higher surface area; however, the coating process resulted in poorer loading efficiencies due to the electrostatic interactions of the beads with the metallic walls of the fluidised bed.

The surface area of cocrystal-coated beads was 4-5 fold higher compared to uncoated beads which can facilitate water uptake and hence, lead to faster release and oral absorption of SDM matching the pharmacokinetic profile of polymorph I generated by milling. In contrast, the same polymorph II generated by spray drying showed a delayed absorption phase due to aggregation in aqueous media as a consequence of having more hydrophobic crystal facets exposed to the media after spray drying [7].

From an industrial point of view, the deposition of the cocrystal as a solid layer onto beads brings two other advantages over powder systems - first, an increase in chemical stability compared to other cocrystal formulations and second, an improvement in flow properties being a formulation that is less sensitive to flow changes during manufacturing processes.

5. Conclusions

Fluidised bed spray coating is a suitable technique for the production of cocrystals deposited as a coating layer onto different substrates. The balance between high loading efficiencies and high degree of crystallinity was optimised when low amounts of binder were used. The cocrystal coated beads have shown an improved *in vitro-in vivo* performance characterised by a faster drug release due to higher surface area leading to enhanced *in vitro* activity and faster

oral absorption and at the same time better chemical stability and flow properties derived from the morphology and solid nature of the starter cores.

Acknowledgments

This publication has emanated from research conducted with the financial support of Science Foundation Ireland under Grant Number SFI/12/RC/2275. We would also like to acknowledge the assistance of Cuspor Limited in generating the accelerated stability prediction models.

Figure captions

Figure 1. Pareto charts depicting the influence of the seven factors (7 bars) assessed on the Taguchi DOE design. Key: a) Degree of crystallinity; b) Loading efficiency and c) Attrition expressed as intact beads recovered after the coating process. Orange bars represent a positive effect of the factor on the response while blue bars represent a negative effect.

Figure 2. 3D response surface (a, b, c) and 2D contour plots (e, f, g) showing the influence of the atomization pressure, the amount of sprayed mass and the amount of binder on the loading efficiency.

Figure 3. 3D response surface (a, b, c) and 2D contour plots (e, f, g) showing the influence of the atomization pressure, the amount of sprayed mass and the amount of binder on the degree of crystallinity.

~~**Figure 4. 3D response surface (a, b, c) and 2D contour plots (e, f, g) showing the influence of the atomization pressure, the amount of sprayed mass and the amount of binder on the yield.**~~

Figure 4. DSC thermograms. A) Effect of binder concentration on 500 µm non-pareil sugar beads. a-Uncoated beads; b-Beads coated with 50% cocrystal:50% PVP; c- Beads coated with 60% cocrystal:40% PVP; d-Beads coated with 70% cocrystal:30% PVP; e-Beads coated with 80% cocrystal:20% PVP; f-Beads coated with 90% cocrystal:10% PVP; g-Beads coated with 95% cocrystal:5% PVP; h- Beads coated with 100% cocrystal:0% PVP. **B) Effect of different types of binder on 500 µm beads.** a- Sugar beads coated with 90% cocrystal:10% Inulin; b- Sugar beads coated with 90% cocrystal:10% PVP; c- Sugar beads coated with 90% cocrystal:10% Eudragit L100-55; d-Sugar beads coated with 90% cocrystal:10% HPMC AS. **C) Effect of 500 µm bead composition.** a- Uncoated microcrystalline beads; b-Microcrystalline beads coated with 95% cocrystal:5% PVP; c- Uncoated sugar beads; d- Sugar beads coated with 95% cocrystal:5% PVP; e—Uncoated tartaric acid beads; f- Tartaric acid beads coated with 95% cocrystal:5% PVP. **D) Effect of bead size and scale-up**. a- 5g-Batch of sugar beads 250 µm coated with 95% cocrystal:5% PVP; b- 5g-Batch of sugar beads 500 µm coated with 95% cocrystal:5% PVP; c- 5g-Batch of sugar beads 1000 µm coated with 95% cocrystal:5% PVP; d- 25g-Batch of sugar beads 250 µm coated with 95% cocrystal:5% PVP; e-25g-Batch of sugar beads 500 µm coated with 95% cocrystal:5% PVP; f- 25g-Batch of sugar beads 1000 µm coated with 95% cocrystal:5% PVP.

Figure 5. DSC thermograms. A) SDM:4ASA cocrystal. a- SDM raw material; b- 4ASA raw material; c-Physical mixture of SDM:4ASA in 1:1 molar ratio; d- 500 µm sugar beads coated with 95% SDM:4ASA cocrystal:5% PVP; e- 500 µm microcrystalline beads coated with 95% SDM:4ASA cocrystal:5% PVP; f-SDM:4ASA cocrystal obtained by spray drying; g-SDM:4ASA cocrystal obtained by solvent evaporation. **B) SDM:NA cocrystal**. a-NA raw material; b- SDM raw material; c- Physical mixture of SDM:NA in 1:1 molar ratio;.d- 500 µm microcrystalline beads coated with 95% SDM:NA cocrystal:5% PVP; e-SDM:NA cocrystal obtained by spray drying. **C) IBU:NAM cocrystal.** a-NAM raw material; b- IBU raw material; c- Physical mixture of IBU:NAM in 1:1 molar ratio; d- 500 µm sugar beads coated with 95% IBU:NAM cocrystal:5% PVP; e-SDM:NA cocrystal obtained by solvent evaporation.

Figure 6. Micrographs of SDM:4ASA cocrystal-coated beads 500 µm. a) Sugar beads coated with 100% cocrystal:0% PVP; b) Sugar beads coated with 95% cocrystal:5% PVP; c) Sugar beads coated with 90% cocrystal:10% PVP; d) Sugar beads coated with 80%

cocrystal:20% PVP; e) Sugar beads coated with 70% cocrystal:30% PVP; f) Sugar beads coated with 60% cocrystal:40% PVP; g) Sugar beads coated with 50% cocrystal:50% PVP; h) Sugar beads coated with 90% cocrystal:10% Inulin; j) Sugar beads coated with 90% cocrystal:10% HPMC AS; k) Sugar beads coated with 90% cocrystal:10% Eudragit; l) Tartaric acid beads coated with 95% cocrystal:5% PVP; m) Microcrystalline cellulose beads coated with 95% cocrystal:5% PVP.

Figure 7. DVS profile and imaging of uncoated and coated non-pareil sugar 1000 µm beads. A) Optical (a1) and SEM image (a2, a3) of uncoated sugar beads; B) Optical (b1) and SEM image (b2, b3) of 5g-Batch of sugar beads coated with 95% cocrystal:5% PVP; C) Optical (c1) and SEM image (c2, c3) 25g-Batch of sugar beads coated with 95% cocrystal:5% PVP; Micrographs 3 correlate with the magnification of the red square of micrographs 2**. D) Moisture sorption (blue line) and desorption (red line) profiles of:** a-uncoated (blank) sugar beads 500 µm, b-5g-Batch of sugar beads 500 µm coated with 95% cocrystal:5% PVP, c- 25g-Batch of sugar beads 500 µm coated with 95% cocrystal:5% PVP**. E) SE** (-♦-) **and SI** (-■-) **values for uncoated beads and 25 g batch 4SDM:4ASA cocrystal coated beads**. Key: U-uncoated, C-coated, S-sugar, M-microcrystalline cellulose, T-tartaric acid, 250- 180-250 µm bead size, 500- 425-500 µm bead size and 1000- 850-1000µm bead size.

Figure 8. A) ***In vitro*** **antimicrobial activity against** ***S. aureus***. In all cases, the efficacy of SDM:4ASA 1:1 molar ratio cocrystal was tested on non-pareil sugar 500 µm beads. Key: SDM, raw material; PM, physical mixture of SDM and 4ASA in 1:1 molar ratio; * $p<0.05$ compared to SDM; # $p<005$ compared to PM. **B and C) SDM:4ASA cocrystal pharmacokinetic profile after single dose oral administration of 15 mg/kg for SDM and 8.3 mg/kg for 4ASA in CD-1 mice.** Formulations tested: Polymorph II cocrystal-coated on non-pareil sugar beads (-▲-), polymorph I cocrystal generated by milling (-■-), polymorph II cocrystal generated by spray drying (-●-) and raw SDM (-▼-). A) SDM plasma concentrations. B) 4ASA plasma concentrations. Statistically significant differences: * = $p < 0.05$ versus SDM; # = $p < 0.05$ versus PII-SD.

References

[1] N.J. Babu, A. Nangia, Solubility Advantage of Amorphous Drugs and Pharmaceutical Cocrystals, Cryst Growth Des, 11 (2011) 2662-2679.
[2] D.R. Serrano, K.H. Gallagher, A.M. Healy, Emerging Nanonisation Technologies: Tailoring Crystalline Versus Amorphous Nanomaterials, Curr Top Med Chem, 15 (2015) 2327-2340.
[3] D.R. Serrano Lopez, A. Lalatsa, Peptide pills for brain diseases? Reality and future perspectives, Ther Deliv, 4 (2013) 479-501.
[4] A.T. Serajuddin, Salt formation to improve drug solubility, Advanced drug delivery reviews, 59 (2007) 603-616.
[5] A.M. Healy, Z.A. Worku, D. Kumar, A.M. Madi, Pharmaceutical solvates, hydrates and amorphous forms: A special emphasis on cocrystals, Adv Drug Deliv Rev, (2017).
[6] C. Grossjohann, D.R. Serrano, K.J. Paluch, P. O'Connell, L. Vella-Zarb, P. Manesiotis, T. McCabe, L. Tajber, O.I. Corrigan, A.M. Healy, Polymorphism in sulfadimidine/4-aminosalicylic acid cocrystals: solid-state characterization and physicochemical properties, Journal of pharmaceutical sciences, 104 (2015) 1385-1398.
[7] D.R. Serrano, T. Persoons, D.M. D'Arcy, C. Galiana, M.A. Dea-Ayuela, A.M. Healy, Modelling and shadowgraph imaging of cocrystal dissolution and assessment of in vitro antimicrobial activity for sulfadimidine/4-aminosalicylic acid cocrystals, Eur J Pharm Sci, 89 (2016) 125-136.
[8] Co-crystal tramadol (hydrochloride) / celecoxib. EMA decision. Available at: http://www.ema.europa.eu/ema/index.jsp?curl=pages/medicines/pips/EMEA-001279-PIP01-12/pip_000910.jsp&mid=WC0b01ac058001d129. Accessed date: 29/04/2017.
[9] C. Almansa, R. Mercè, N. Tesson, J. Farran, J. Tomàs†, C.R. Plata-Salamán, Co-crystal of Tramadol Hydrochloride–Celecoxib (ctc): A Novel API–API Co-crystal for the Treatment of Pain, Cryst. Growth Des, 17 (2017) 1884-1892.
[10] A. Alhalaweh, W. Kaialy, G. Buckton, H. Gill, A. Nokhodchi, S.P. Velaga, Theophylline cocrystals prepared by spray drying: physicochemical properties and aerosolization performance, AAPS PharmSciTech, 14 (2013) 265-276.
[11] D.R. Serrano, P. O'Connell, K.J. Paluch, D. Walsh, A.M. Healy, Cocrystal habit engineering to improve drug dissolution and alter derived powder properties, J Pharm Pharmacol, 68 (2016) 665-677.
[12] N. Kolasinac, K. Kachrimanis, J. Djuris, I. Homsek, B. Grujic, S. Ibric, Spray coating as a powerful technique in preparation of solid dispersions with enhanced desloratadine dissolution rate, Drug Dev Ind Pharm, 39 (2013) 1020-1027.
[13] R.R. Namburi, J.E. Kerr, Oral itraconazole formulations and methods of making the same, in: D.I.A. B.V (Ed.), USA, 2003.
[14] S. Beg, G. Sharma, K. Thanki, S. Jain, O.P. Katare, B. Singh, Positively charged self-nanoemulsifying oily formulations of olmesartan medoxomil: Systematic development, in vitro, ex vivo and in vivo evaluation, Int J Pharm, 493 (2015) 466-482.
[15] B. Guebitz, H. Schnedl, J.G. Khinast, A risk management ontology for Quality-by Design based on a new development approach according GAMP 5.0. , Expert Syst Appl 39 (2012) 7291-7301.
[16] F.L.F. Soares, R.L. Carneiro, Green Synthesis of Ibuprofen−Nicotinamide Cocrystals and In-Line Evaluation by Raman Spectroscopy Cryst. Growth Des, 13 (2013) 1510-1517.
[17] M. Rolon, D.R. Serrano, A. Lalatsa, E. de Pablo, J.J. Torrado, M.P. Ballesteros, A.M. Healy, C. Vega, C. Coronel, F. Bolas-Fernandez, M.A. Dea-Ayuela, Engineering Oral and Parenteral Amorphous Amphotericin B Formulations against Experimental Trypanosoma cruzi Infections, Mol Pharm, 14 (2017) 1095-1106.

[18] V. Curtin, Y. Amharar, K.H. Gallagher, S. Corcoran, L. Tajber, O.I. Corrigan, A.M. Healy, Reducing mechanical activation-induced amorphisation of salbutamol sulphate by co-processing with selected carboxylic acids, International journal of pharmaceutics, 456 (2013) 508-516.
[19] D.R. Serrano, N.A. Mugheirbi, P. O'Connell, N. Leddy, A.M. Healy, L. Tajber, The impact of substrate properties on the formation of spherulitic films: a case study of salbutamol sulfate, Cryst. Growth Des, 16 (2016) 3853-3858.
[20] A.S. Narang, V. Sheverev, T. Freeman, D. Both, V. Stepaniuk, M. Delancy, D. Millington-Smith, K. Macias, G. Subramanian, Process Analytical Technology for High Shear Wet Granulation: Wet Mass Consistency Reported by In-Line Drag Flow Force Sensor Is Consistent With Powder Rheology Measured by At-Line FT4 Powder Rheometer, J Pharm Sci, 105 (2016) 182-187.
[21] S.P. Chaudhari, R.H. Dave, To prepare and characterize microcrystalline cellulose granules using water and isopropyl alcohol as granulating agents and determine its end-point by thermal and rheological tools, Drug Dev Ind Pharm, 41 (2015) 744-752.
[22] D.R. Serrano, A. Lalatsa, M.A. Dea-Ayuela, P.E. Bilbao-Ramos, N.L. Garrett, J. Moger, J. Guarro, J. Capilla, M.P. Ballesteros, A.G. Schatzlein, F. Bolas, J.J. Torrado, I.F. Uchegbu, Oral particle uptake and organ targeting drives the activity of amphotericin B nanoparticles, Mol Pharm, 12 (2015) 420-431.
[23] S. Bianco, F. Tewes, L. Tajber, V. Caron, O.I. Corrigan, A.M. Healy, Bulk, surface properties and water uptake mechanisms of salt/acid amorphous composite systems, Int J Pharm, 456 (2013) 143-152.
[24] K.C. Waterman, The application of the Accelerated Stability Assessment Program (ASAP) to quality by design (QbD) for drug product stability, AAPS PharmSciTech, 12 (2011) 932-937.
[25] K.C. Waterman, J.T. Swanson, B.L. Lippold, A scientific and statistical analysis of accelerated aging for pharmaceuticals. Part 1: accuracy of fitting methods, J Pharm Sci, 103 (2014) 3000-3006.
[26] E.S. Darwish, A.M. Abdel Fattah, F.A. Attaby, O.N. Al-Shayea, Synthesis and Antimicrobial Evaluation of Some Novel Thiazole, Pyridone, Pyrazole, Chromene, Hydrazone Derivatives Bearing a Biologically Active Sulfonamide Moiety, Int. J. Mol. Sci., 15 (2014) 1237-1254.
[27] United States Pharmacopeia and National Formulary, United States Pharmacopeial Convention Inc., Rockville, MD, USA, 26th Edition, (2008).
[28] Y. Zhang, M. Huo, J. Zhou, S. Xie, PKSolver: An add-in program for pharmacokinetic and pharmacodynamic data analysis in Microsoft Excel, Comput Methods Programs Biomed, 99 (2010) 306-314.
[29] D.R. Serrano, L. Hernandez, L. Fleire, I. Gonzalez-Alvarez, A. Montoya, M.P. Ballesteros, M.A. Dea-Ayuela, G. Miro, F. Bolas-Fernandez, J.J. Torrado, Hemolytic and pharmacokinetic studies of liposomal and particulate amphotericin B formulations, Int J Pharm, 447 (2013) 38-46.
[30] A. Shukla, V. Mishra, B.S. Bhoop, O.P. Katare, Alginate coated chitosan microparticles mediated oral delivery of diphtheria toxoid. Part A. Systematic optimization, development and characterization, International journal of pharmaceutics, 495 (2015) 220-233.
[31] V. Caron, L. Tajber, O.I. Corrigan, A.M. Healy, A comparison of spray drying and milling in the production of amorphous dispersions of sulfathiazole/polyvinylpyrrolidone and sulfadimidine/polyvinylpyrrolidone, Mol Pharm, 8 (2011) 532-542.
[32] M.M. Knopp, N.E. Olesen, P. Holm, P. Langguth, R. Holm, T. Rades, Influence of Polymer Molecular Weight on Drug-Polymer Solubility: A Comparison between

Experimentally Determined Solubility in PVP and Prediction Derived from Solubility in Monomer, J Pharm Sci, 104 (2015) 2905-2912.
[33] D.D. Gadade, S.S. Pekamwar, Pharmaceutical Cocrystals: Regulatory and Strategic Aspects, Design and Development, Advanced pharmaceutical bulletin, 6 (2016) 479-494.
[34] D.P. Kale, S.S. Zode, A.K. Bansal, Challenges in Translational Development of Pharmaceutical Cocrystals, J Pharm Sci, 106 (2017) 457-470.
[35] A. Alhalaweh, S.P. Velaga, Formation of Cocrystals from Stoichiometric Solutions of Incongruently Saturating Systems by Spray Drying, Cryst. Growth Des, 10 (2010) 3302-3305.
[36] A.N. Manin, A.P. Voronin, A.V. Shishkina, M.V. Vener, A.V. Churakov, G.L. Perlovich, Influence of Secondary Interactions on the Structure, Sublimation Thermodynamics, and Solubility of Salicylate:4-Hydroxybenzamide Cocrystals. Combined Experimental and Theoretical Study, The journal of physical chemistry. B, 119 (2015) 10466-10477.
[37] K. Muzaffar, G.A. Nayik, P. Kumar, Stickiness Problem Associated with Spray Drying of Sugar and Acid Rich Foods: A Mini Review., J Nutr Food Sci S12 (2015) 1-3.
[38] A. Ziaee, A.B. Albadarin, L. Padrela, A. Faucher, E. O'Reilly, G. Walker, Spray drying ternary amorphous solid dispersions of ibuprofen – An investigation into critical formulation and processing parameters, Eur J Pharm Biopharm, 120 (2017) 43-51.
[39] M.A. Mohammad, A. Alhalaweh, S.P. Velaga, Hansen solubility parameter as a tool to predict cocrystal formation, Int J Pharm, 407 (2011) 63-71.
[40] A. Forster, J. Hempenstall, I. Tucker, T. Rades, Selection of excipients for melt extrusion with two poorly water-soluble drugs by solubility parameter calculation and thermal analysis, Int J Pharm, 226 (2001) 147-161.
[41] D. Walsh, D.R. Serrano, Z.A. Worku, B.A. Norris, A.M. Healy, Production of Cocrystals in an Excipient Matrix by Spray Drying, International Journla of Pharmaceutics, (Under revision) (2017).
[42] N. Kolašinac, K. Kachrimanis, J. Djuriš, I. Homšek, B. Grujić, S. Ibrić, Spray coating as a powerful technique in preparation of solid dispersions with enhanced desloratadine dissolution rate, Drug Dev Ind Pharm, 39 (2013) 1020-1027.
[43] S. Rehder, M. Klukkert, K.A. Lobmann, C.J. Strachan, A. Sakmann, K. Gordon, T. Rades, C.S. Leopold, Investigation of the Formation Process of Two Piracetam Cocrystals during Grinding, Pharmaceutics, 3 (2011) 706-722.
[44] A. Jayasankar, A. Somwangthanaroj, Z.J. Shao, N. Rodriguez-Hornedo, Cocrystal formation during cogrinding and storage is mediated by amorphous phase, Pharm Res, 23 (2006) 2381-2392.
[45] N. Kallai, O. Luhn, J. Dredan, K. Kovacs, M. Lengyel, I. Antal, Evaluation of drug release from coated pellets based on isomalt, sugar, and microcrystalline cellulose inert cores, AAPS PharmSciTech, 11 (2010) 383-391.
[46] N.A. Mugheirbi, P. O'Connell, D.R. Serrano, A.M. Healy, L.S. Taylor, L. Tajber, A Comparative Study on the Performance of Inert and Functionalized Spheres Coated with Solid Dispersions Made of Two Structurally Related Antifungal Drugs, Mol Pharm, 14 (2017) 3718-3728.
[47] J.J. Sousa, A. Sousa, M.J. Moura, F. Podczeck, J.M. Newton, The influence of core materials and film coating on the drug release from coated pellets, Int J Pharm, 233 (2002) 111-122.

Figure 1

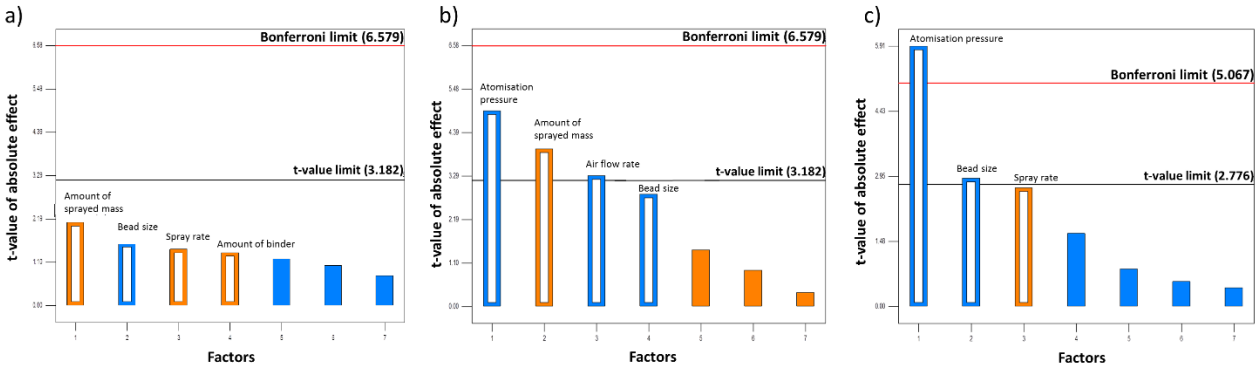
a)
Bonferroni limit (6.579)
t-value limit (3.182)
Amount of sprayed mass
Bead size
Spray rate
Amount of binder
t-value of absolute effect
Factors
b)
Bonferroni limit (6.579)
Atomisation pressure
Amount of sprayed mass
Air flow rate
Bead size
t-value limit (3.182)
t-value of absolute effect
Factors
c)
Atomisation pressure
Bonferroni limit (5.067)
Bead size
Spray rate
t-value limit (2.776)
t-value of absolute effect
Factors

Figure 2

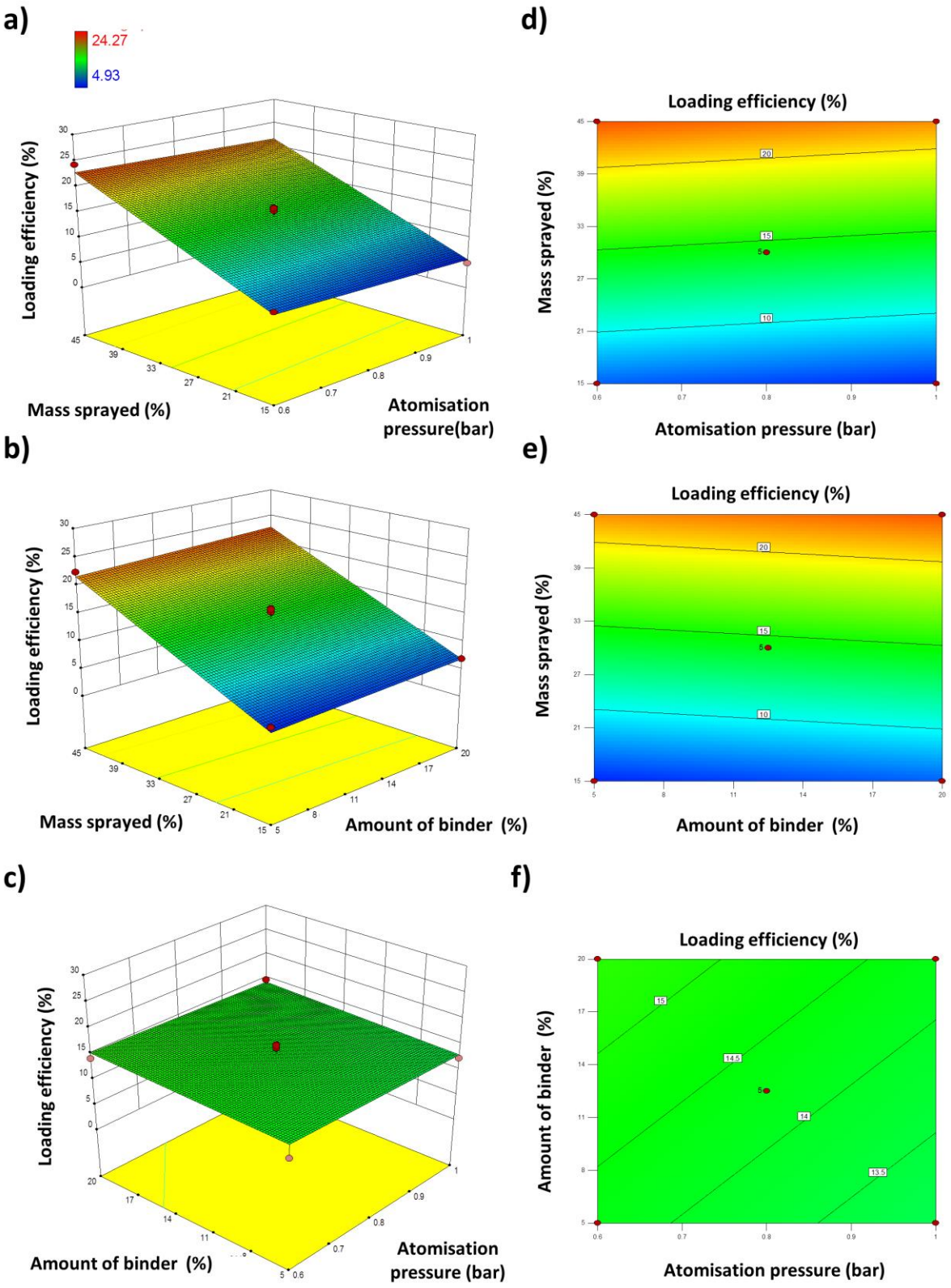
a)
24.27
4.93
Loading efficiency (%)
Mass sprayed (%)
Atomisation pressure(bar)
d)
Loading efficiency (%)
Mass sprayed (%)
Atomisation pressure (bar)
b)
Loading efficiency (%)
Mass sprayed (%)
Amount of binder (%)
e)
Loading efficiency (%)
Mass sprayed (%)
Amount of binder (%)
c)
Loading efficiency (%)
Amount of binder (%)
Atomisation pressure (bar)
f)
Loading efficiency (%)
Amount of binder (%)
Atomisation pressure (bar)

Figure 3

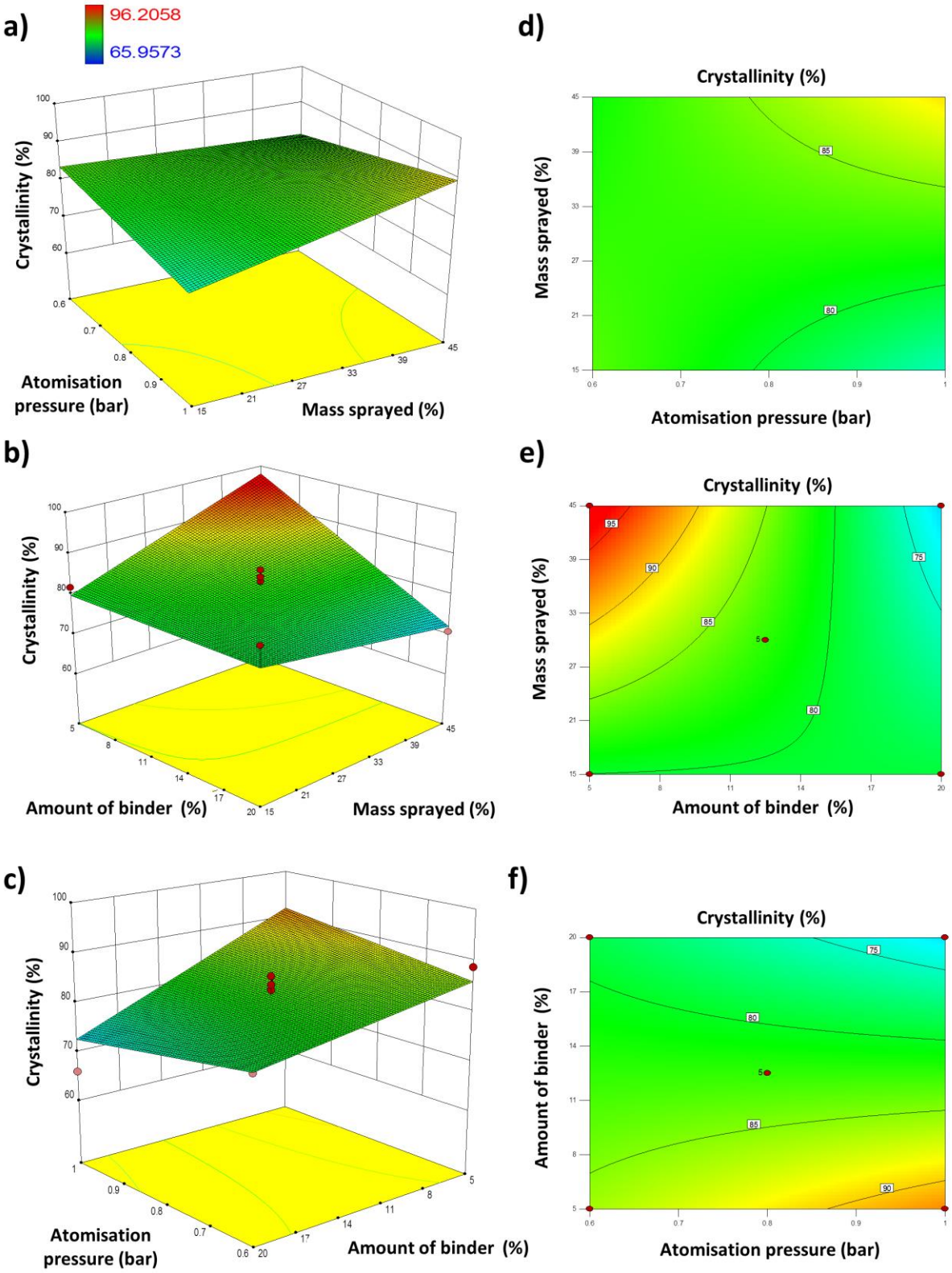
a)
96.2058
65.9573
Crystallinity (%)
Atomisation pressure (bar)
Mass sprayed (%)
b)
Crystallinity (%)
Amount of binder (%)
Mass sprayed (%)
c)
Crystallinity (%)
Atomisation pressure (bar)
Amount of binder (%)
d)
Crystallinity (%)
Mass sprayed (%)
Atomisation pressure (bar)
e)
Crystallinity (%)
Mass sprayed (%)
Amount of binder (%)
f)
Crystallinity (%)
Amount of binder (%)
Atomisation pressure (bar)

Figure 4

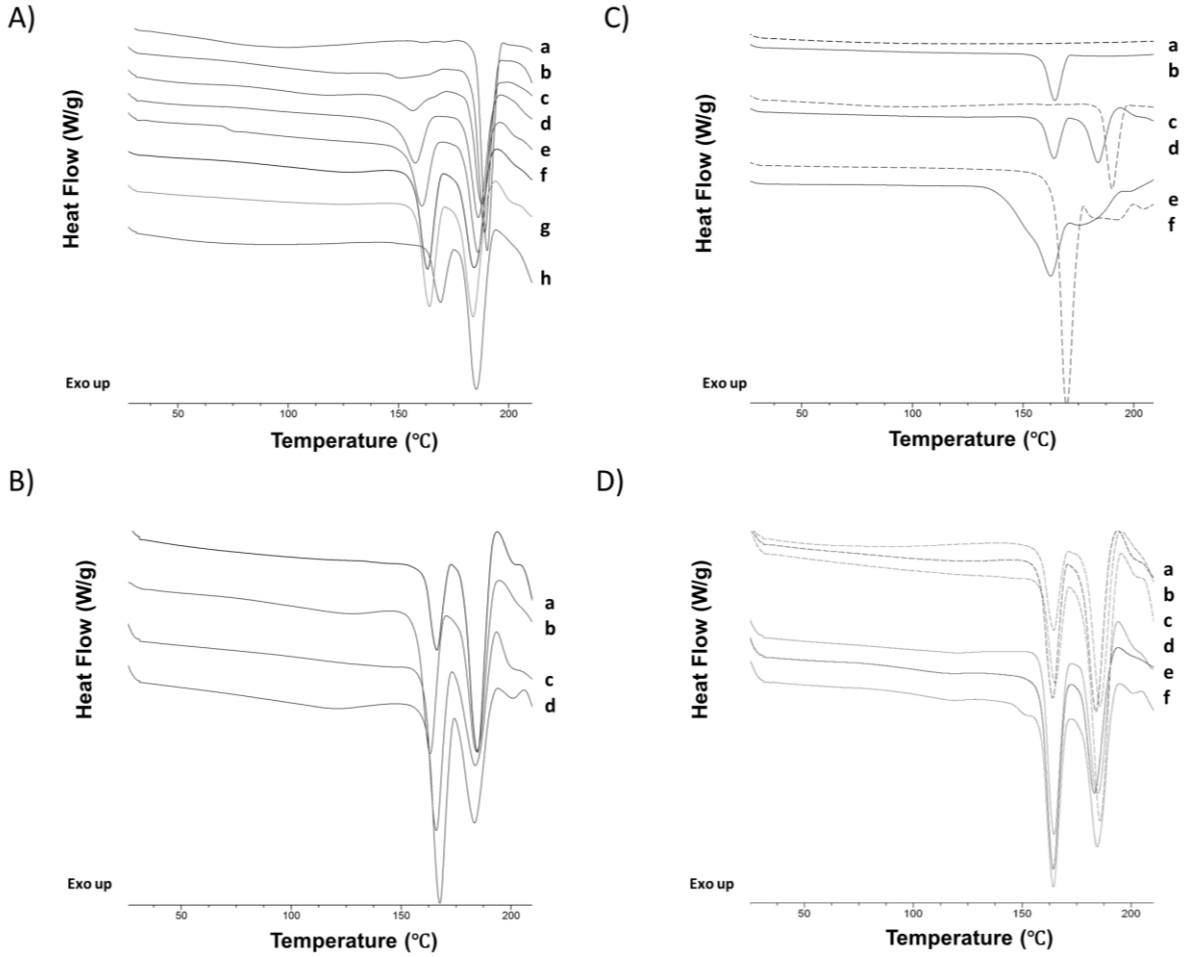
A)
Heat Flow (W/g)
a
b
c
d
e
f
g
h
Exo up
50
100
150
200
Temperature (℃)
C)
Heat Flow (W/g)
a
b
c
d
e
f
Exo up
50
100
150
200
Temperature (℃)
B)
Heat Flow (W/g)
a
b
c
d
Exo up
50
100
150
200
Temperature (℃)
D)
Heat Flow (W/g)
a
b
c
d
e
f
Exo up
50
100
150
200
Temperature (℃)

Figure 5

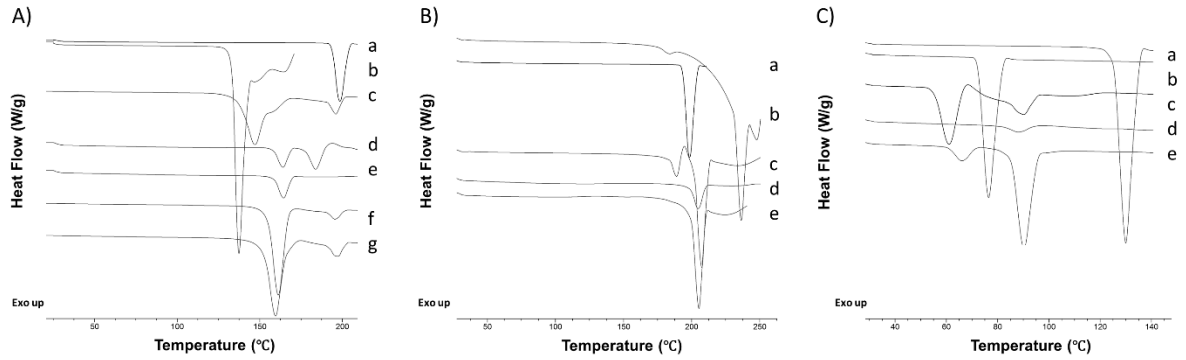
A)
Heat Flow (W/g)
a
b
c
d
e
f
g
Exo up
50
100
150
200
Temperature (℃)
B)
Heat Flow (W/g)
a
b
c
d
e
Exo up
50
100
150
200
250
Temperature (℃)
C)
Heat Flow (W/g)
a
b
c
d
e
Exo up
40
60
80
100
120
140
Temperature (℃)

Figure 6

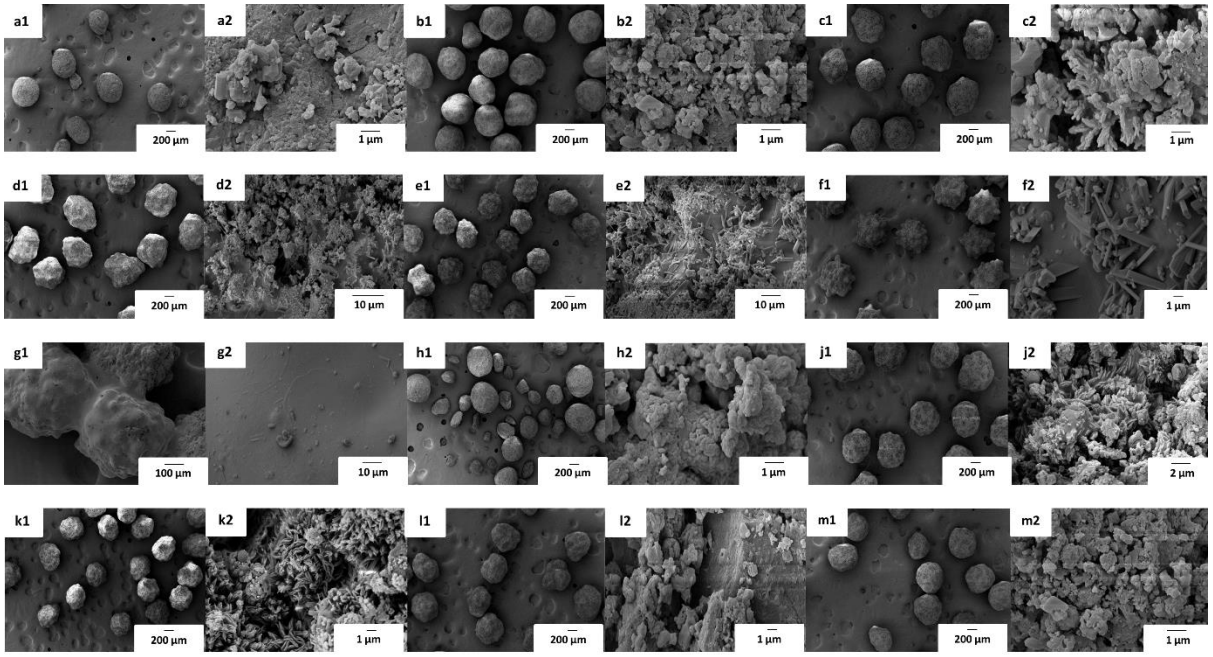
a1
200 µm
a2
1 µm
b1
200 µm
b2
1 µm
c1
200 µm
c2
1 µm
d1
200 µm
d2
10 µm
e1
200 µm
e2
10 µm
f1
200 µm
f2
1 µm
g1
100 µm
g2
10 µm
h1
200 µm
h2
1 µm
j1
200 µm
j2
2 µm
k1
200 µm
k2
1 µm
l1
200 µm
l2
1 µm
m1
200 µm
m2
1 µm

Figure 7

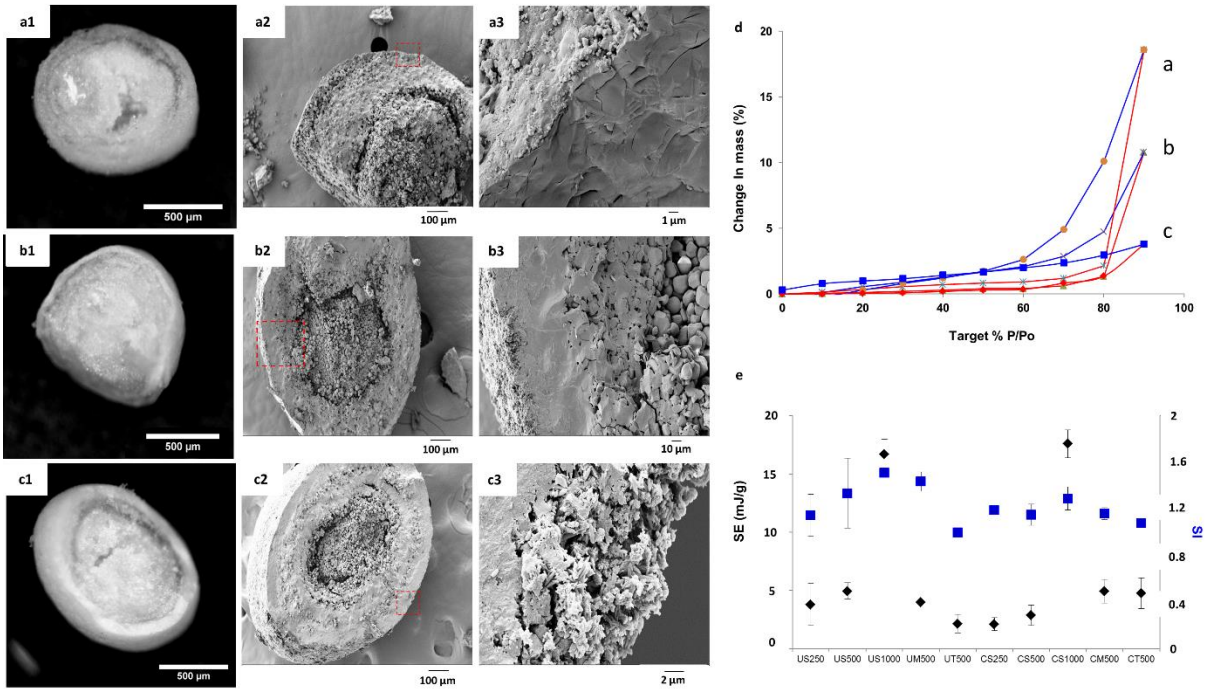
a1
a2
a3
500 µm
100 µm
1 µm
b1
b2
b3
500 µm
100 µm
10 µm
c1
c2
c3
500 µm
100 µm
2 µm
d
Change In mass (%)
Target % P/Po
a
b
c
e
SE (mJ/g)
SI
US250
US500
US1000
UM500
UT500
CS250
CS500
CS1000
CM500
CT500

Figure 8

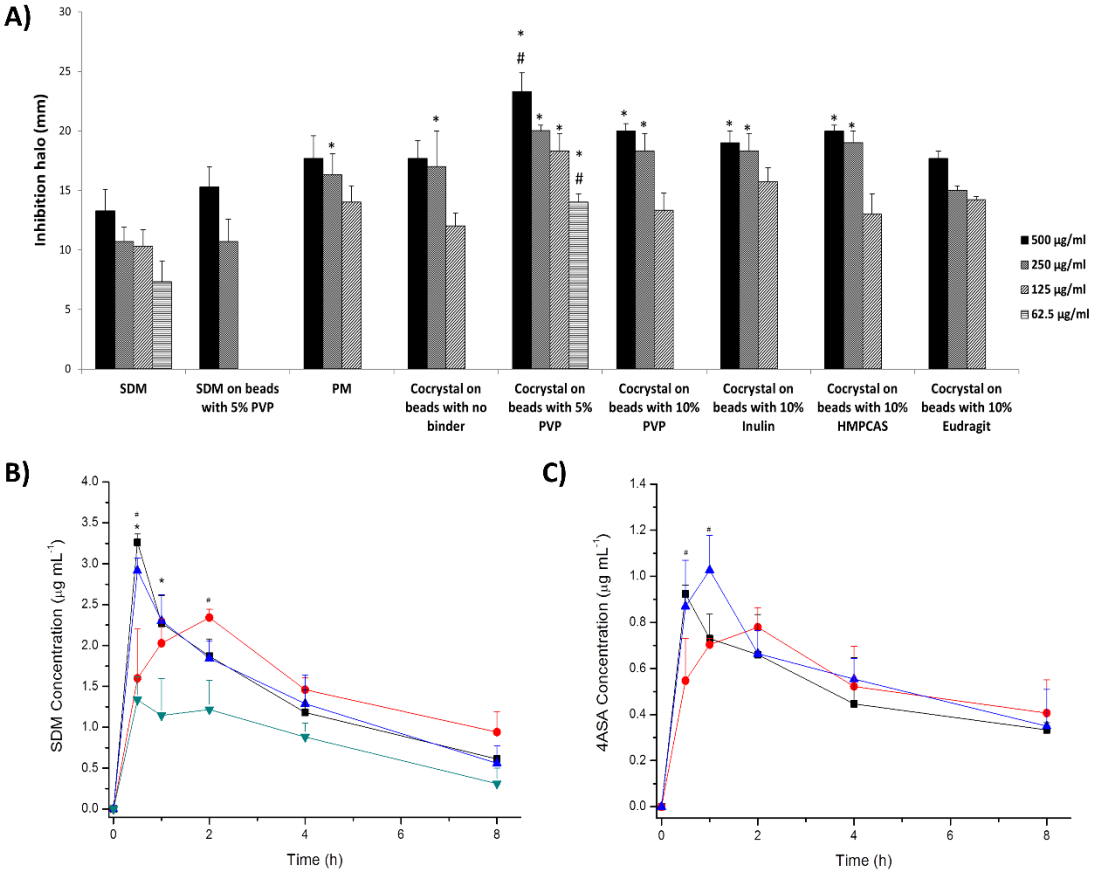
A)
Inhibition halo (mm)
500 µg/ml
250 µg/ml
125 µg/ml
62.5 µg/ml
SDM
SDM on beads with 5% PVP
PM
Cocrystal on beads with no binder
Cocrystal on beads with 5% PVP
Cocrystal on beads with 10% PVP
Cocrystal on beads with 10% Inulin
Cocrystal on beads with 10% HMPCAS
Cocrystal on beads with 10% Eudragit
B)
SDM Concentration (µg mL-1)
Time (h)
C)
4ASA Concentration (µg mL-1)
Time (h)

SUPPLEMENTARY MATERIAL

Optimising the *in vitro* and *in vivo* performance of oral cocrystal formulations via spray coating

Dolores R. Serrano[a,b,c*], David Walsh[a,b], Peter O'Connell[a], Naila A. Mugheirbi[d], Zelalem Ayenew Worku[a,b], Francisco Bolas-Fernandez[c], Carolina Galiana[e], Maria Auxiliadora Dea-Ayuela[e], Anne Marie Healy[a,b]

[a]School of Pharmacy and Pharmaceutical Sciences, Trinity College Dublin, Dublin 2, Ireland.
[b]SSPC, Synthesis and Solid State Pharmaceutical Centre, Ireland.
[c]School of Pharmacy, Universidad Complutense de Madrid, Plaza Ramón y Cajal s/n, 28040-Madrid, Spain.
[d]Department of Industrial and Physical Pharmacy, Purdue University, West Lafayette, IN 47907-2091, USA.
[e]Departamento de Farmacia, Facultad de Ciencias de la Salud, Universidad CEU Cardenal Herrera, Edificio Seminario s/n, 46113-Moncada, Valencia, Spain

*Corresponding authors:

Dolores R. Serrano
Department of Pharmaceutical Technology
School of Pharmacy
Universidad Complutense de Madrid
Plaza Ramon y Cajal s/n
28040-Madrid, Spain.
Email: drserran@ucm.es

Anne Marie Healy
School of Pharmacy and Pharmaceutical Sciences
Trinity College Dublin
Dublin 2, Ireland.
Tel.: +353 1 896 1444
E-mail address: healyam@tcd.ie

Table S1. Target product profile (TPP) elements for cocrystal-coated inert cores.

TPP Elements	Target	Justification
Dosage form (capsules)	Cocrystal-coated on inert cores	Cocrystal engineering can enhance the oral bioavailability of poorly bioavailable drug such as sulfadimidine
Route of administration	Oral	Recommended route for delivery of sulfadimidine for the management of antimicrobial infection
Dosage type	Fast release	Faster onset of action leading to enhanced oral bioavailability and consequently fast drug dissolution is required
Pharmacokinetics	Higher C_{max} and AUC	Required for achieving higher drug levels into the blood stream to enhance therapeutic action
Packaging	Capsules	Coated inert cores can be easily packed in capsules for improved patient compliance portability and ease of manufacturing due to good powder flowability
Stability	At least 24 months at room temperature	To maintain drug efficacy during storage period. Cocrystals ensures higher storage stability than amorphous dispersions.

Table S2. Critical quality attributes (CQAs) for cocrystal-coated inert cores containing SDM and rational justification.

Critical Quality Attributes		Target	Is this a CQA?	Rational justification
Physical attributes	**Colour**	Acceptable to patients	No	Colour, odour and appearance were not considered as critical, as these are not directly linked to patient efficacy and safety.
	Odour	No unpleasant odour		
	Appearance	Acceptable to patients		
Content uniformity (RSD, %)		≤ 1%	Yes	Content uniformity affect drug safety and efficacy, for this reason a homogeneous cocrystal-coating layer was considered as moderately critical.
Drug release in 30 min (%)		≥50%	Yes	*In vitro* dissolution performance of the dosage form, during early dissolution phase is considered critical as will dictate the pharmacokinetic profile and efficacy of the drug.
Crystallinity content (%)		≥ 90%	Yes	Percentage of crystallinity is regarded highly critical as determines the solid state and stability of the drug and creation of unintentional co-amorphous should be minimised.
Loading efficiency (%)		≥ 20%	Yes	Loading efficiency should be maximised as the amount of SDM administered in patients is moderately high.

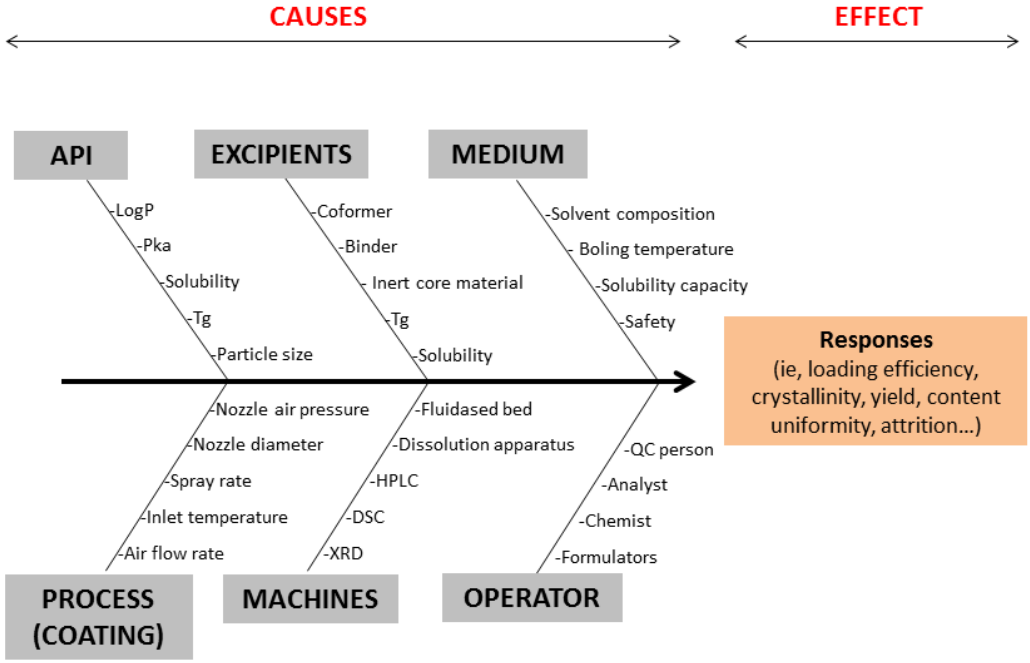

Figure S1. Ishikawa fish-bone diagram depicting various causes and sub-causes affecting the spray coating process.

Table S3. Model generation and predicted equations obtained from the Box-Behnken DoE.

Model (p-value)	**Predicted equation in terms of actual factors**
Two factor interaction (p< 0.01)	**Crystallinity**= +79.17 -15.24*Atomisation pressure- 0.21*Amount of mass sprayed +2.43*Amount of binder +1.36*Atomisation pressure*Amount of mass sprayed -2.04*Atomisation pressure*Amount of binder -0.06*Amount of mass sprayed*Amount of binder
Linear (< 0.0001)	**Loading efficiency**= -0.36 -2.87*Atomisation pressure +0.53*Amount of mass sprayed +0.08*Amount of binder
Two factor interaction (p< 0.12)	**Attrition**= -39.17 -59.16*Atomisation pressure -0.98*Amount of mass sprayed -0.04*Amount of binder -1.47*Atomisation pressure*Amount of mass sprayed -0.03*Atomisation pressure*Amount of binder +0.003*Amount of mass sprayed*Amount of binder
Linear (p<0.03)	**Yield**= -101.08 -11.28*Atomisation pressure -0.47*Amount of mass sprayed -0.21*Amount of binder
Linear (p<0.09)	**Log10(RSD)**= +0.63 +0.17*Atomisation pressure -0.03*Amount of mass sprayed -0.002*Amount of binder

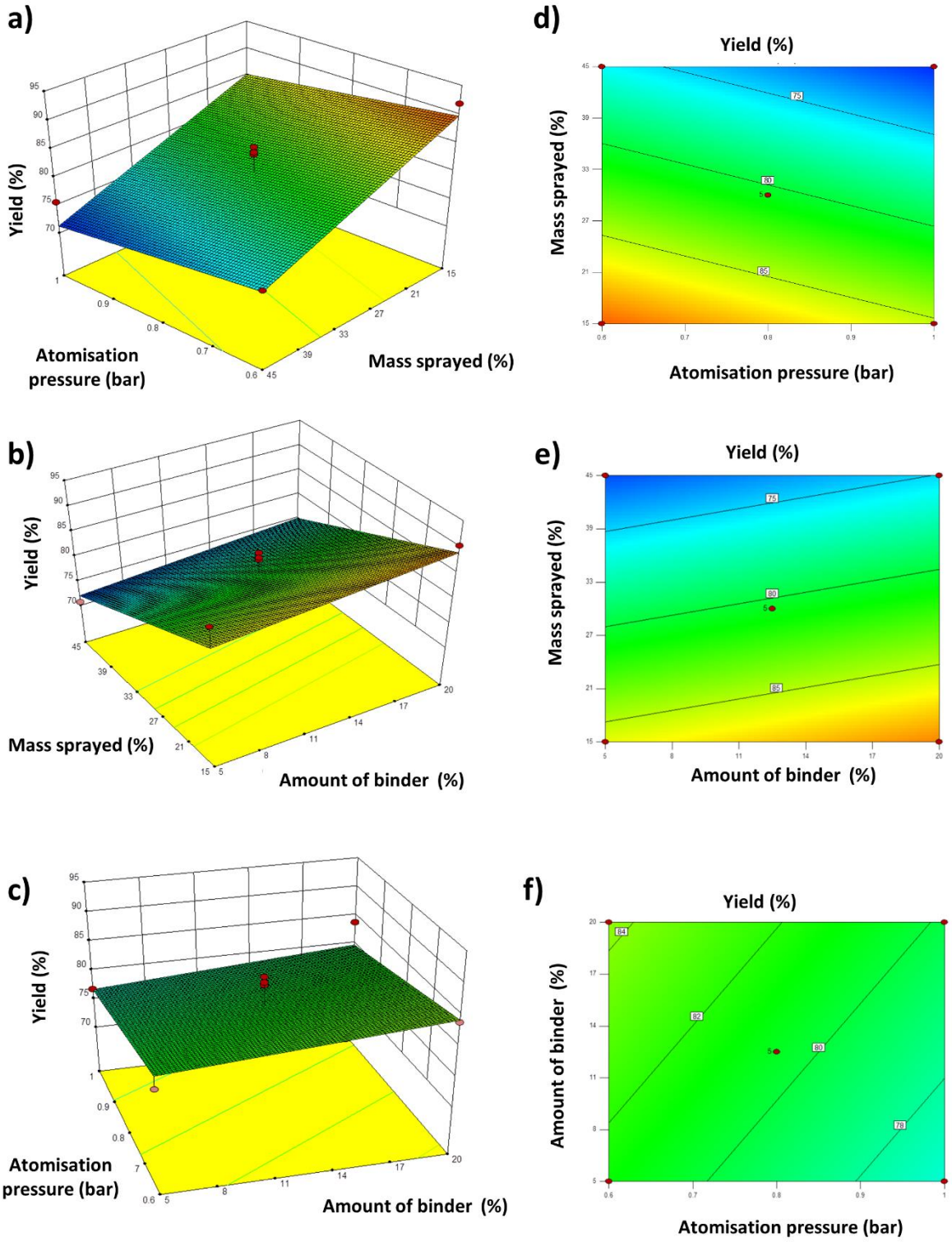

Figure 2SA. 3D response surface (a, b, c) and 2D contour plots (e, f, g) showing the influence of the atomization pressure, the amount of sprayed mass and the amount of binder on the yield.

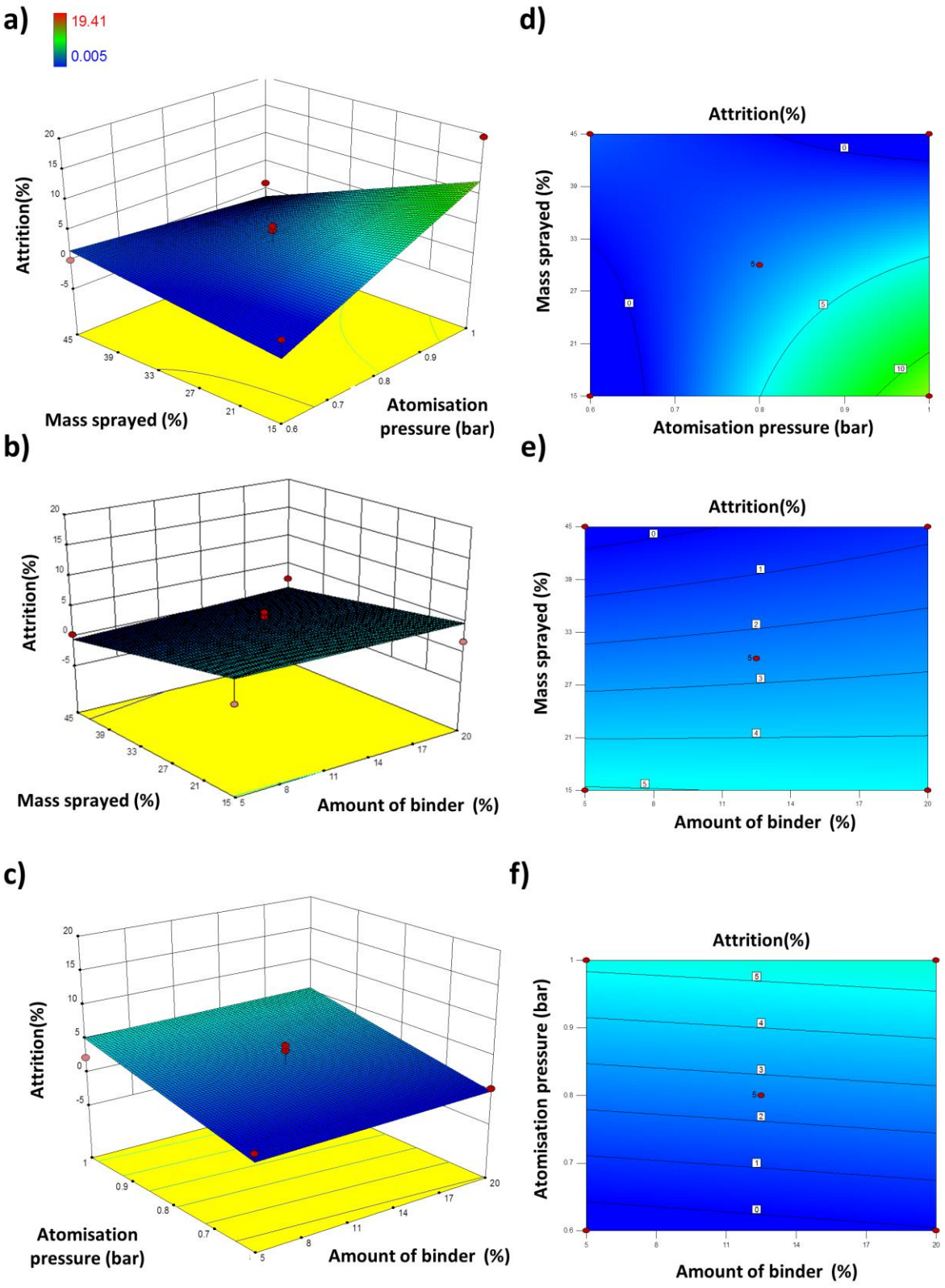

Figure S2B. 3D response surface (a, b, c) and 2D contour plots (e, f, g) showing the influence of the atomization pressure, the amount of sprayed mass and the amount of binder on the percentage of attrition.

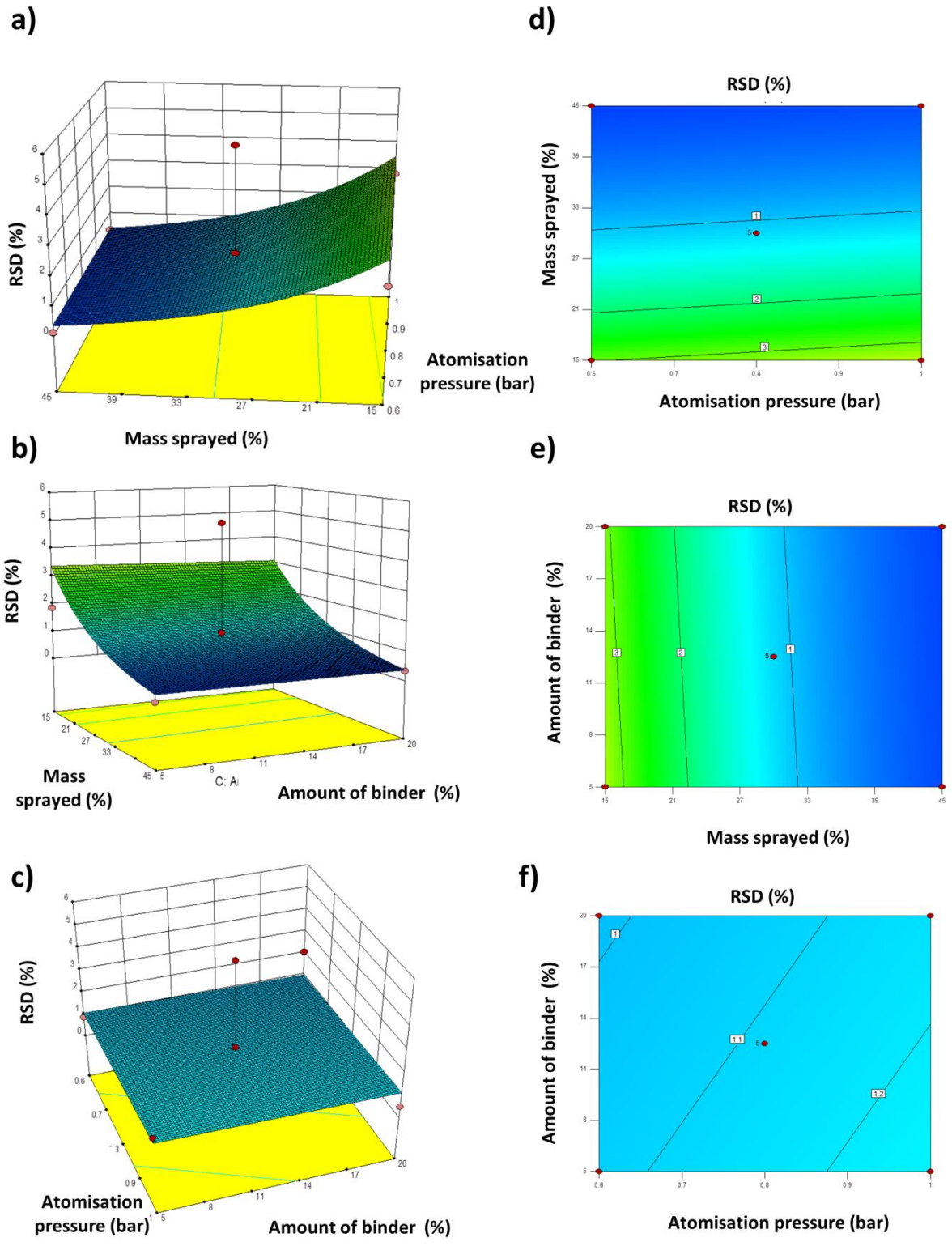

Figure S3. 3D response surface (a, b, c) and 2D contour plots (e, f, g) showing the influence of the atomization pressure, the amount of sprayed mass and the amount of binder on content uniformity (RSD).

Table S4. **Results of numeric optimization of cocrystal-coated beads.**

	Constrains (Goals)	Lower limit	Upper limit
Factors			
Amount of binder (%)	In range	-1	+1
Amount of sprayed mass (%)	In range	-1	+1
Atomisation pressure (Bar)	In range	-1	+1
Response			
Loading efficiency (%)	Maximisation	4.9	24.7
Degree of crystallization (%)	Maximisation	65.9	96.0
Yield (%)	In range	70.5	91.9
Attrition (%)	In range	0.01	19.41
RSD (%)	In range	0.03	5.09
Optimised formulation			
Amount of binder (%)	5	-	-
Amount of sprayed mass (%)	45	-	-
Atomisation pressure (Bar)	0.75	-	-

Table S5. Comparison of experimental results with predicted responses. Key: CI, Confidence intervals.

Response	Experimental Results					Predicted results			
	Experiment Run 1	Experiment Run 2	Experiment Run 3	Mean	SD	Predicted	Percent Error	95% CI low	95% CI high
Loading efficiency (%)	22.51	22.11	20.50	21.71	1.06	22.07	1.06	19.54	24.61
Degree of crystallinity (%)	93.48	97.47	94.49	95.15	2.07	96.21	0.76	87.99	104.41

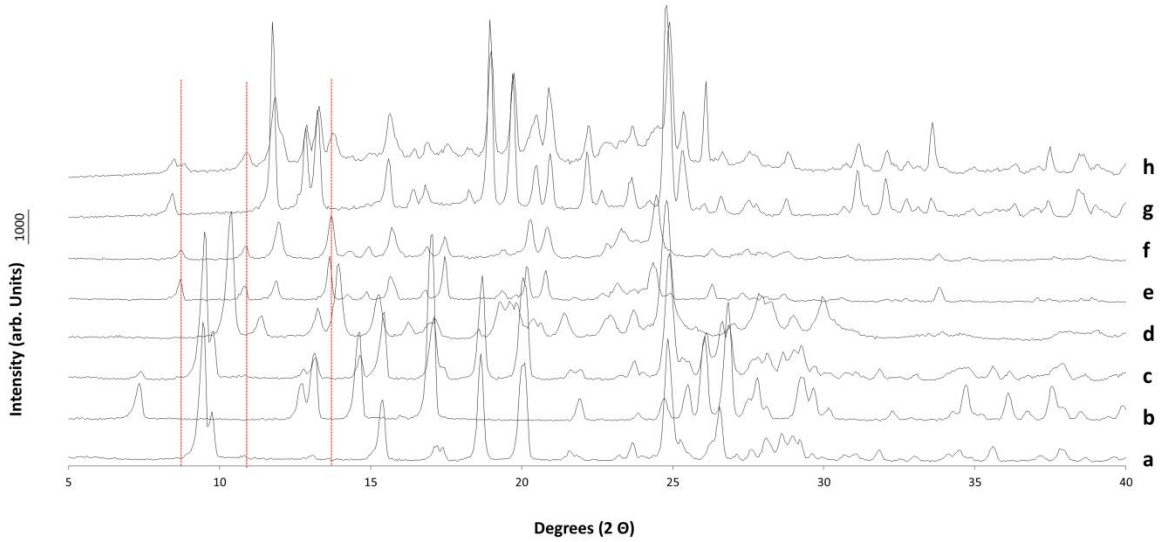

Figure S4. XRD patterns. Key: a- SDM raw material; b- 4ASA raw material; c-Physical mixture of SDM:4ASA (1:1 molar ratio); d- SDM:4ASA polymorph I generated by milling; e- SDM:4ASA polymorph II generated by solvent evaporation; f- SDM:4ASA polymorph II generated by spray drying; g- Blank non-pareil sugar 500 µm beads; h- SDM-4ASA cocrystal polymorph II coated on non-pareil sugar 500 µm beads.

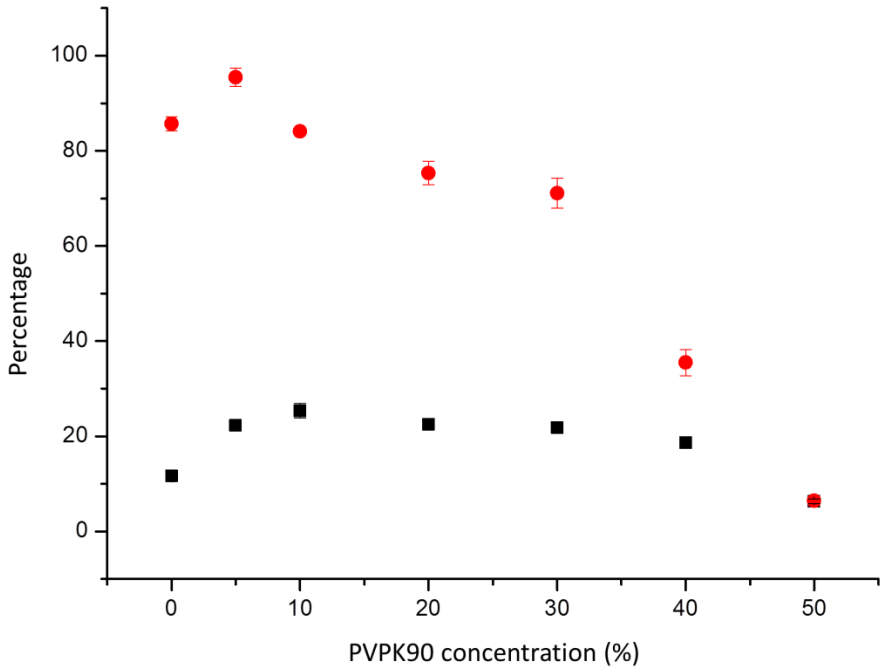

Figure S5. Effect of PVPK90 concentration on cocrystal formation during spray coating. Key: The percentage of the degree of crystallinity and loading efficiency are represented in red and black respectively.

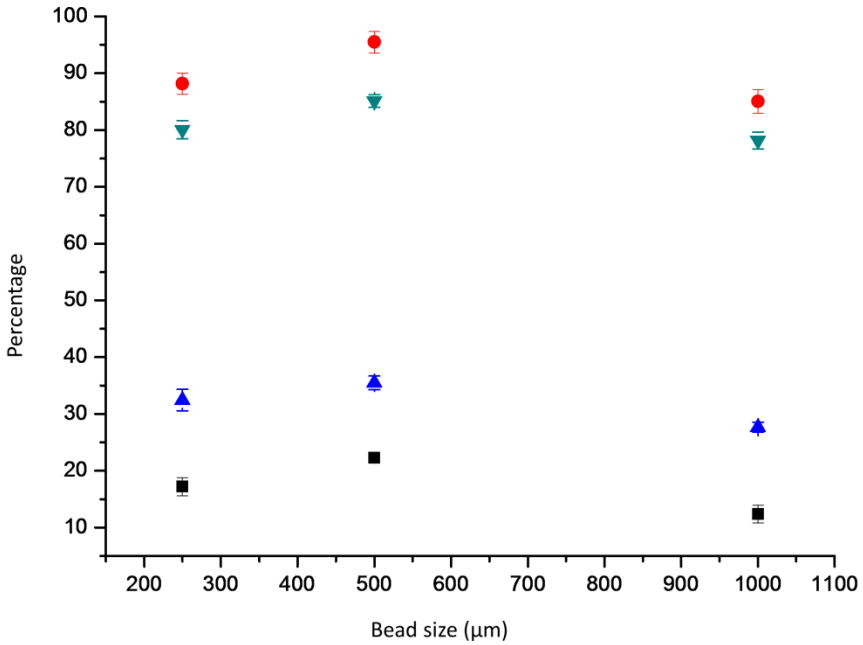

Figure S6. Effect of bead and batch size on cocrystal formation during spray coating. Key: The percentage of the degree of crystallinity and loading efficiency for the 5 g batch size are represented in red and black respectively and for the 25 g batch size in green and blue.

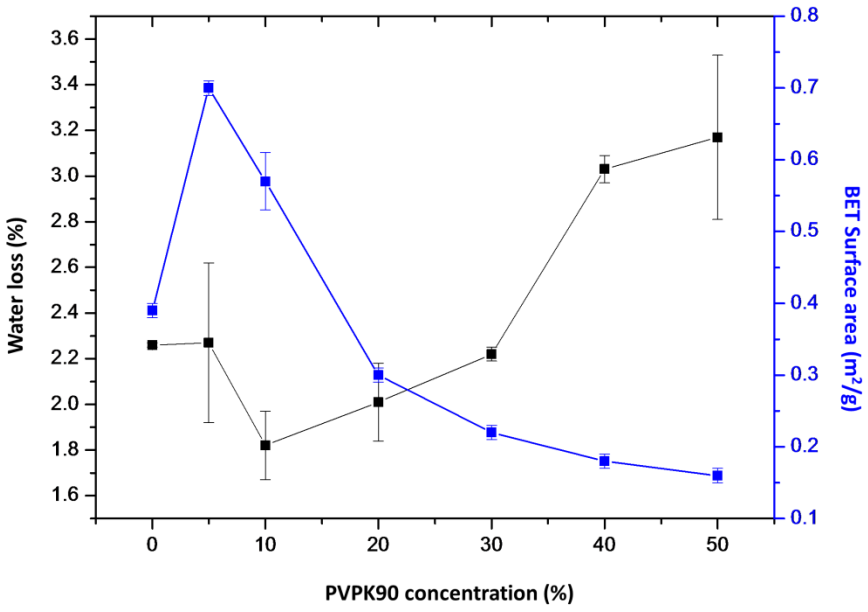

Figure S7. Effect of PVPK90 concentration on water content and surface area during spray coating.

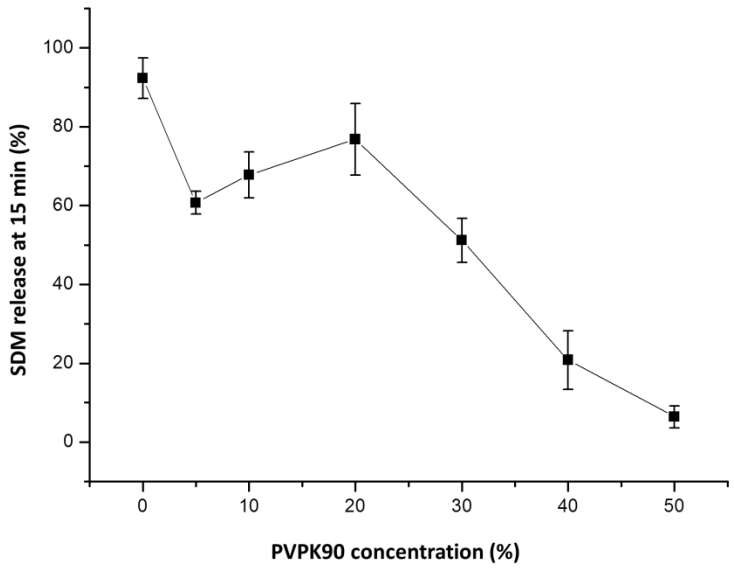

Figure S8. Effect of PVPK90 concentration on the SDM release.

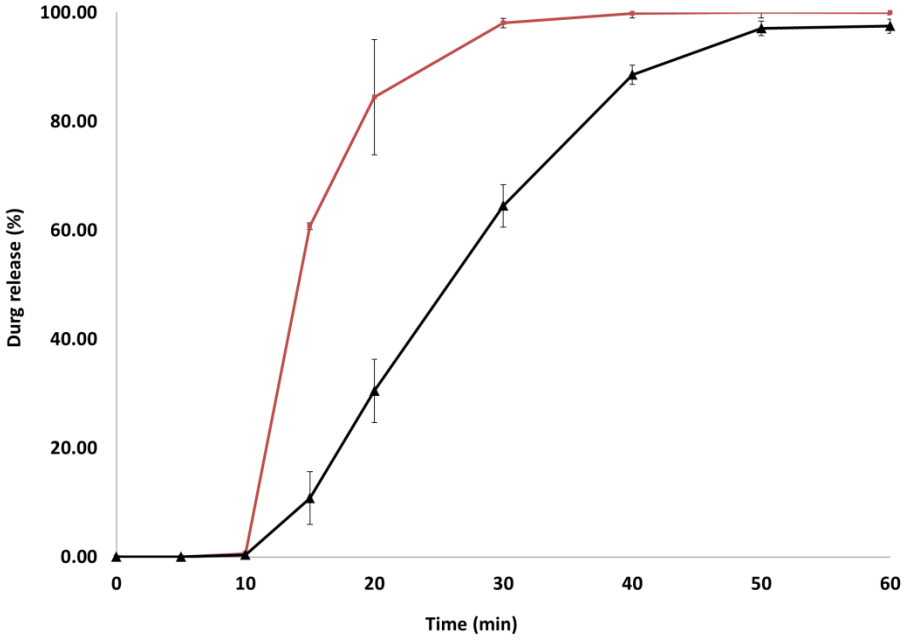

Figure S9. Dissolution profile of SDM:4ASA cocrystal coated beads (in red) versus SDM coated beads (in black).

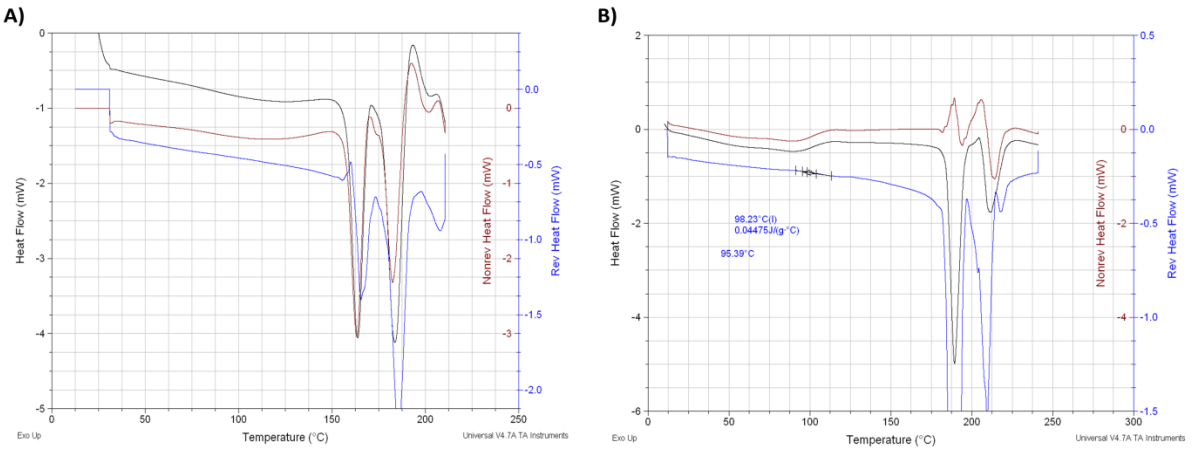

Figure S10. MTDSC thermograms of SDM:4ASA cocrystal coated beads (A) and SDM-PVP coated beads (B). The glass transition can be observed in the reversing heat flow signal (blue line).

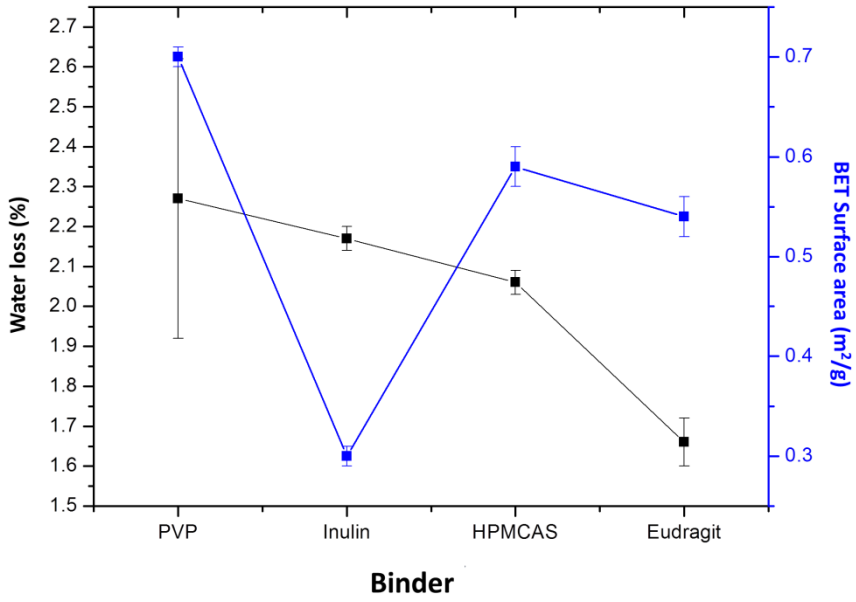

Figure S11. Effect of the type of binder on water content and surface area during spray coating.

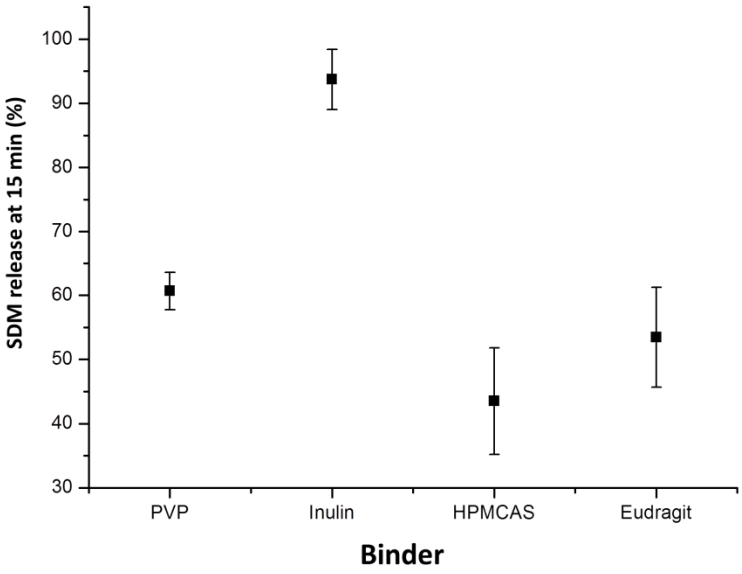

Figure S12. Effect of the type of binder on the SDM release.

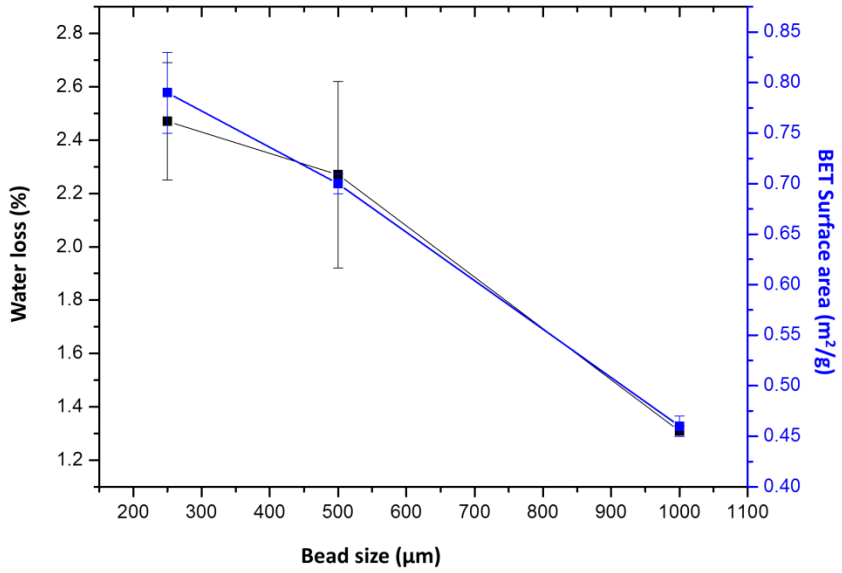

Figure S13. Effect of the bead size on water content and surface area during spray coating.

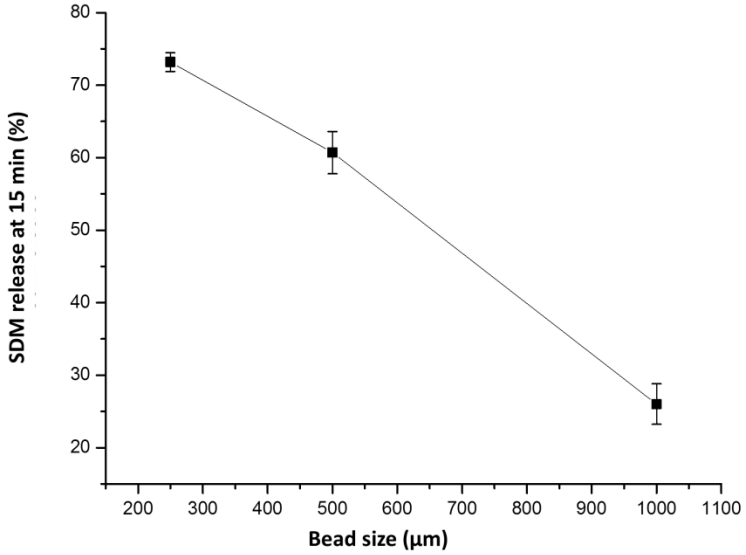

Figure S14. Effect of the bead size on the SDM release.

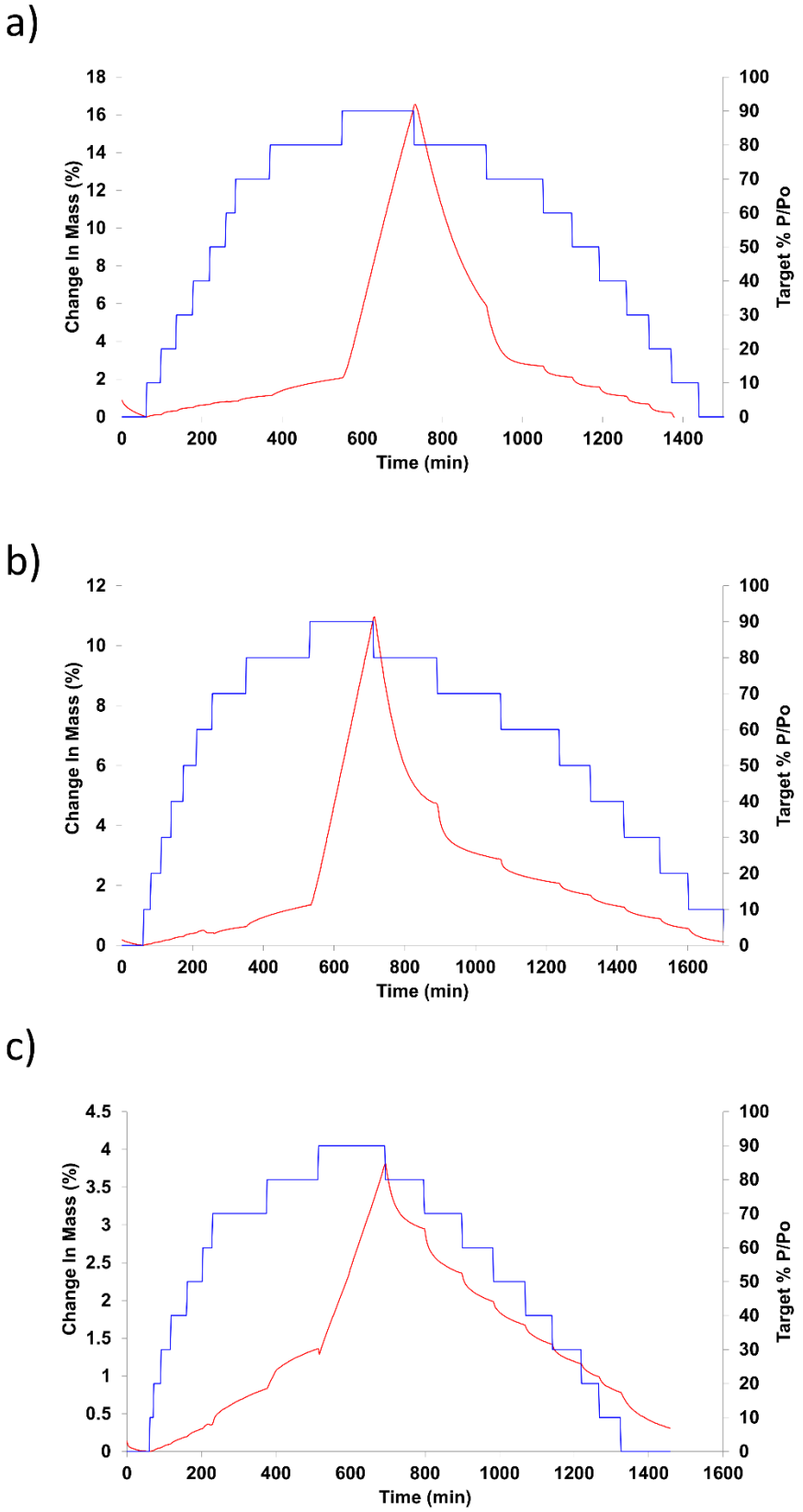

Figure S15. DVS sorption and desorption profile of: a) uncoated (blank) sugar beads 500 µm; b) 5g-Batch of sugar beads 500 µm coated with 95% cocrystal:5% PVP and c) 25g-Batch of sugar beads 500 µm coated with 95% cocrystal:5% PVP.

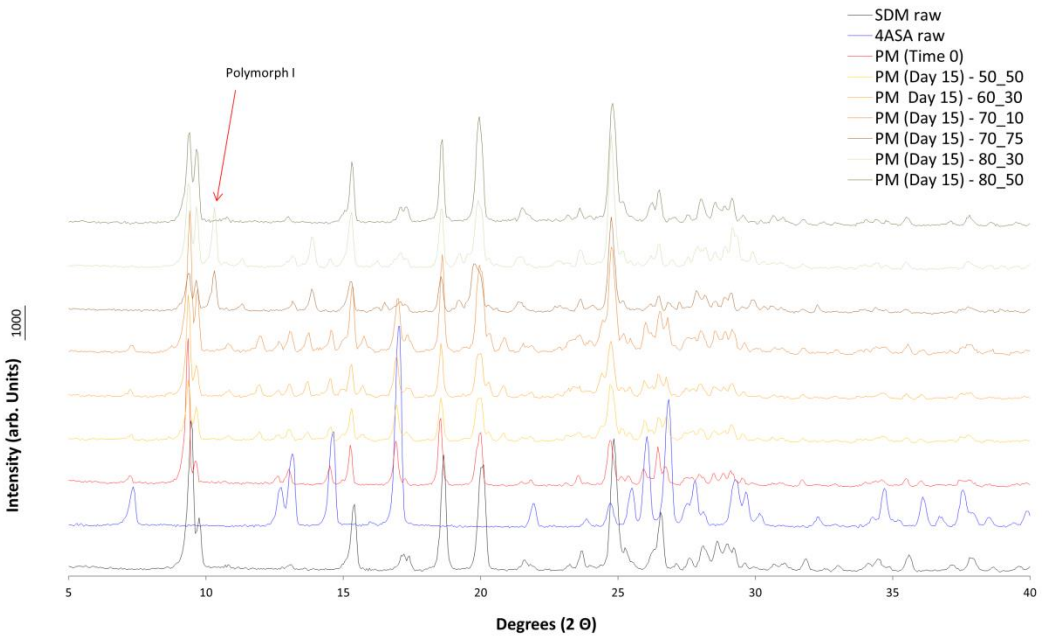

Figure S16. PXRD patterns of SDM:4ASA physical mixture at different times during the accelerated stability studies.

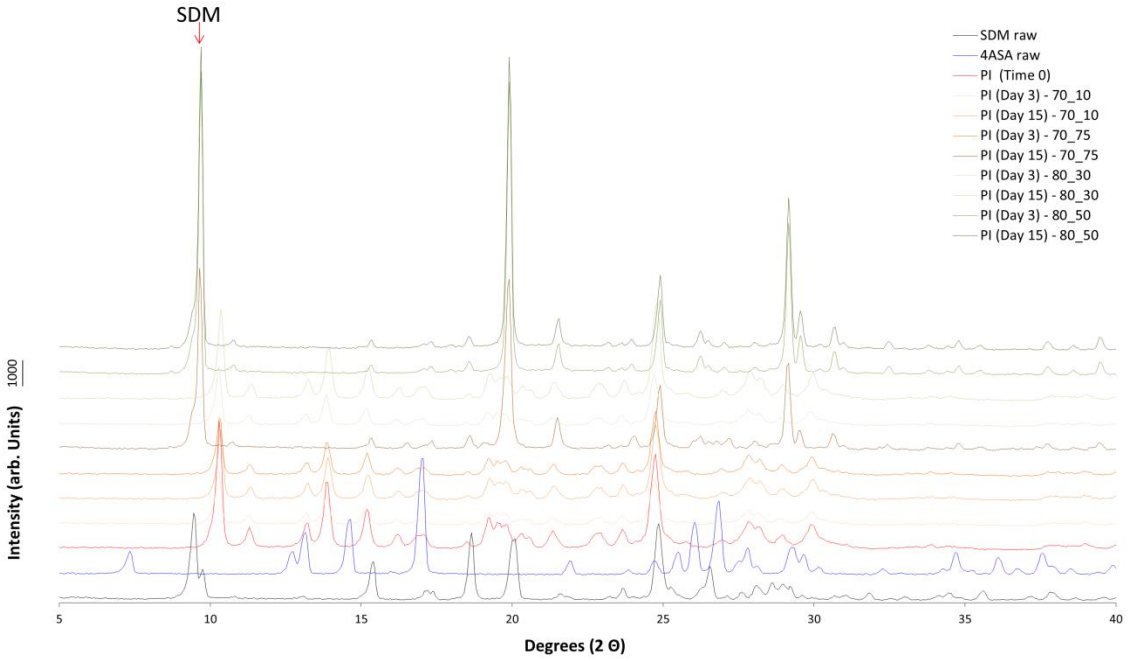

Figure S17. PXRD patterns of SDM:4ASA polymorph I at different times during the accelerated stability studies.

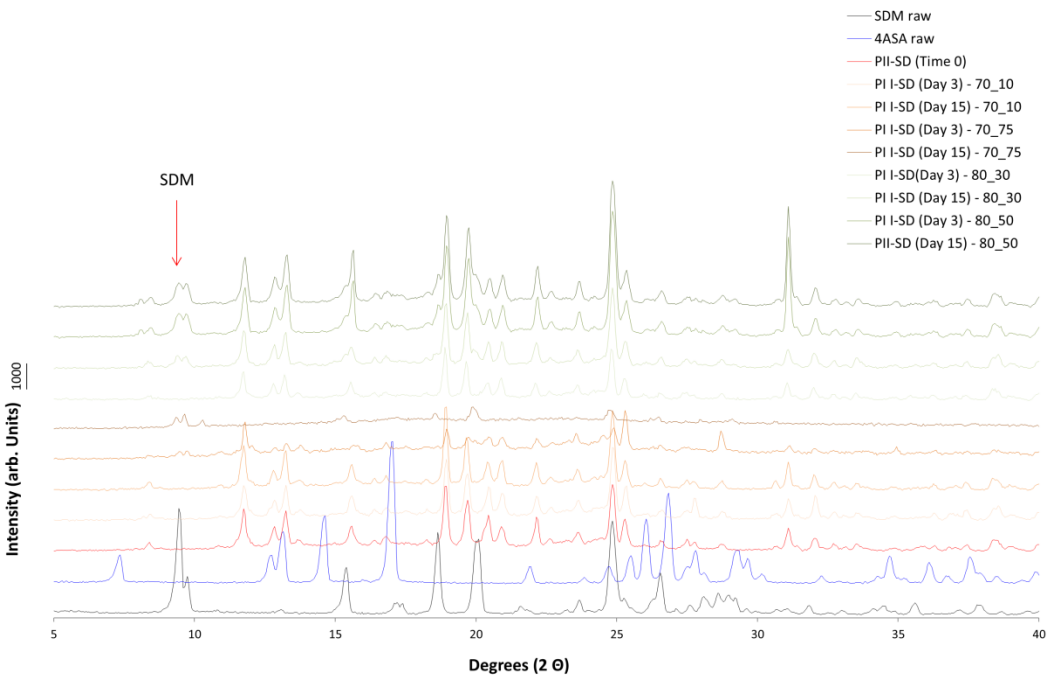

Figure S18. PXRD patterns of SDM:4ASA polymorph II generated by spray-drying at different times during the accelerated stability studies.